Excited-State Photodynamics of Perylene−Porphyrin Dyads. 5. Tuning Light-Harvesting Characteristics via Perylene Substituents, Connection Motif, and Three-Dimensional Architecture†

Christine Kirmaier,‡ Hee-eun Song,‡ Eunkyung Yang,‡ Jennifer K. Schwartz,‡ Eve Hindin,‡ James R. Diers,§ Robert S. Loewe,|| Kin-ya Tomizaki,|| Fabien Chevalier,|| Lavoisier Ramos, Robert R. Birge,⊥ Jonathan S. Lindsey,*,|| David F. Bocian,*,§ and Dewey Holten*,‡

Department of Chemistry, Washington University, St. Louis, Missouri, 63130-4889, Department of Chemistry, University of California, Riverside, California, 92521-0403, Department of Chemistry, North Carolina State University, Raleigh, North Carolina, 27695-8204, and Department of Chemistry, University of Connecticut, Storrs, Connecticut, 06269-3060

Received: November 10, 2009; Revised Manuscript Received: December 20, 2009

Seven perylene−porphyrin dyads were examined with the goal of identifying those most suitable for components of light-harvesting systems. The ideal dyad should exhibit strong absorption by the perylene in the green, undergo rapid and efficient excited-state energy transfer from perylene to porphyrin, and avoid electron-transfer quenching of the porphyrin excited state by the perylene in the medium of interest. Four dyads have different perylenes at the *p*-position of the *meso*-aryl group on the zinc porphyrin. The most suitable perylene identified in that set was then incorporated at the *m*- or *o*-position of the zinc porphyrin, affording two other dyads. An analogue of the *o*-substituted architecture was prepared in which the zinc porphyrin was replaced with the free base porphyrin. The perylene in each dyad is a monoimide derivative; the perylenes differ in attachment of the linker (either via a diphenylethyne linker at the *N*-imide or an ethynylphenyl linker at the C9 position) and the number (0−3) of 4-*tert*-butylphenoxy groups (which increase solubility and slightly alter the electrochemical potentials). In the *p*-linked dyad, the monophenoxy perylene with an *N*-imide diphenylethyne linker is superior in providing rapid and essentially quantitative energy transfer from excited perylene to zinc porphyrin with minimal electron-transfer quenching in both toluene and benzonitrile. The dyads with the same perylene at the *m*- or *o*-position exhibited similar results except for one case, the *o*-linked dyad bearing the zinc porphyrin in benzonitrile, where significant excited-state quenching is observed; this phenomenon is facilitated by close spatial approach of the perylene and porphyrin and the associated thermodynamic/kinetic enhancement of the electron-transfer process. Such quenching does not occur with the free base porphyrin because electron transfer is thermodynamically unfavorable even in the polar medium. The *p*-linked dyad containing a zinc porphyrin attached to a bis(4-*tert*-butylphenoxy)perylene via an ethynylphenyl linker at the C9 position exhibits ultrafast and quantitative energy transfer in toluene; the same dyad in benzonitrile exhibits ultrafast (<0.5 ps) perylene-to-porphyrin energy transfer, rapid (∼5 ps) porphyrin-to-perylene electron transfer, and fast (∼25 ps) charge recombination to the ground state. Collectively, this study has identified suitable perylene−porphyrin constructs for use in light-harvesting applications.

I. Introduction

Multipigment arrays that absorb visible light and funnel the resulting excited-state energy rapidly and efficiently to a designated site are of great interest for probing the mechanisms of electronic energy migration among pigments[1] and may provide the basis for new types of molecular constructs for solar-energy applications. Among various pigments, members of the porphyrin family are attractive candidates for light-harvesting systems due to their high absorption coefficients and facile excited-state energy-transfer characteristics. In this regard, the energy-transfer characteristics for a wide variety of multiporphyrin arrays have been examined.[2] Although porphyrins absorb blue light quite strongly, they have rather limited absorption across the remainder of the visible spectrum. Improvements in the overall light-harvesting efficiency can be realized by the introduction of accessory pigments.

The ideal features[3] of an accessory pigment for use with porphyrins appear to be largely satisfied by perylene-imide chromophores, which exhibit the following attributes: (1) perylene-imides absorb light strongly in the region between the porphyrin Soret and Q bands.[4] (2) A perylene-imide typically displays a long and monophasic singlet excited-state lifetime,[5] and typically has a fluorescence quantum yield near unity.[6,7] (3) Perylene-imides are exceptionally stable.[6] (4) Perylene-imides can be derivatized with synthetic handles in a variety of ways for use in modular building-block approaches.[8–10]

The literature concerning perylene is vast ("perylene" itself elicits >4000 citations on Web of Science). A key focus for

‡ Washington University.
§ University of California, Riverside.
|| North Carolina State University.
⊥ University of Connecticut.
† Part of the "Michael R. Wasielewski Festschrift".
* To whom correspondence should be addressed. E-mail: holten@wuchem.wustl.edu (D.H.); David.Bocian@ucr.edu (D.F.B); jlindsey@ncsu.edu (J.S.L.).

10.1021/jp910705q

CHART 1: Previously Studied Perylene-imides

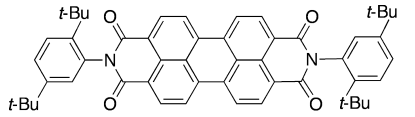

PDI-m (two isomers)

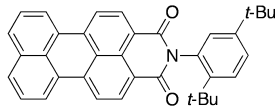

PMI-1

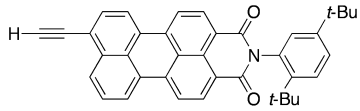

PMI-e

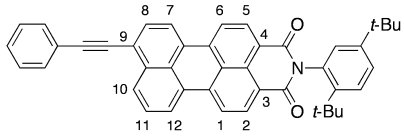

PMI-ep
(including numbering system)

CHART 2: Perylene-monoimides Studied Herein

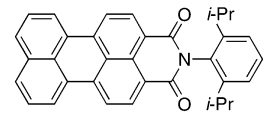

PMI-2

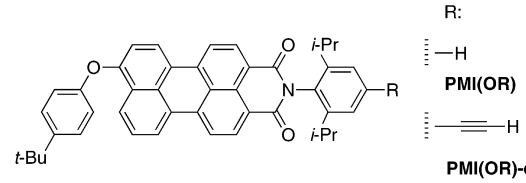

PMI(OR)
PMI(OR)-e

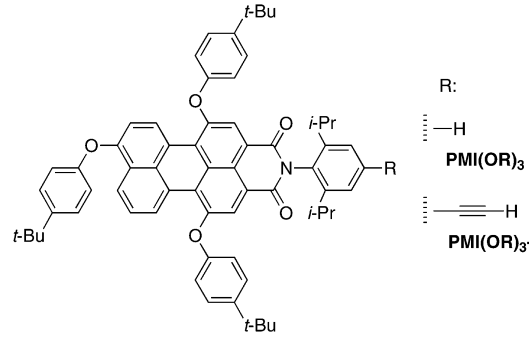

PMI(OR)$_3$
PMI(OR)$_3$-e

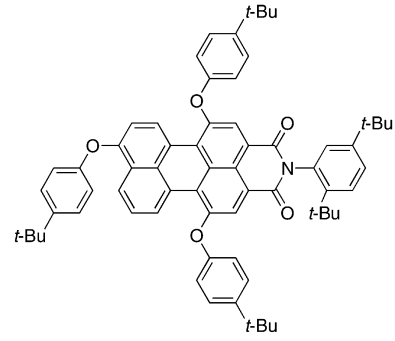

PMI(OR)$_3$-1

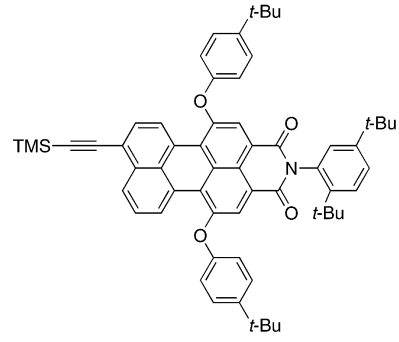

PMI(OR)$_2$-e-TMS

much work with perylene-imides concerns perylene-bisimides, which are excellent electron acceptors and, with appropriate *N*-imide substituents, readily aggregate to give higher-order assemblies.[11] Far less work has been carried out with perylene-monoimides, which are much poorer electron acceptors but still aggregate in the absence of solubilizing substituents.[12] Representative perylene-bisimide and perylene-monoimides are **PDI-m** and **PMI-1**, respectively, shown in Chart 1.

Both types of perylene-imides have strong absorption ($\varepsilon_{\lambda max}$ $\sim$50 000 $M^{-1}cm^{-1}$) in the region between the porphyrin Soret and Q bands. Introduction of bulky groups at the *N*-aryl moieties is necessary to achieve solubility. For example, the perylene bearing *tert*-butyl groups on the aryl rings (**PDI-m**) is readily soluble in organic solvents, whereas the analogue (not shown) with unsubstituted phenyl substituents is not.[13] The *N*-aryl group can also be substituted with 2,6-diisopropyl groups as a means of achieving high solubility, as shown for perylene-monoimide **PMI-2** and other perylene-monoimides examined herein (Chart 2).[14] The absorption and emission characteristics of the perylene-imides are little affected by the presence of solubilizing substituents at the imide position because of the nodes present at the imide nitrogen in both the HOMO and LUMO.[15,16] Further increases in solubility are achieved upon introduction of alkoxy substituents directly at the perimeter of the perylene nucleus.[8–10] On the other hand, the introduction of alkoxy groups for solubilization (Chart 2) or 9-ethynyl groups for joining with dyads (e.g., **PMI-e** in Chart 1) also results in bathochromic shifts in the absorption spectrum.

A substantial amount of prior work has been done concerning arrays composed of tetrapyrrole macrocycles and perylene-imides,[17–23] with the focus also chiefly centering on perylene-bisimides, whereupon the perylene serves as an electron acceptor upon photoexcitation and often directs formation of higher-order assemblies. In our own work, we have prepared a large number of dyads and multads composed of tetrapyrrole macrocycles and perylene-imides.[24–35] In each case, the perylene-imide was derivatized with bulky substituents to achieve high solubility in organic solvents, thereby suppressing self-aggregation. Initial studies concerned dyads containing a porphyrin and a perylene-bisimide.[24,25] To achieve efficient energy transfer with minimal competing electron transfer, we then focused on perylene-monoimides containing bulky substituents.[24,27–31,33] Although synthetic access to perylene-monoimides initially was limited, scalable routes have since been developed that provide robust entrée to perylene-monoimide building blocks.[35]

Chart 3 displays two such dyad motifs containing a porphyrin and a perylene-imide, as well as benchmark porphyrins for comparison purposes. One dyad utilizes a perylene-bisimide (PDI) joined to the porphyrin at the *N*-imide position of the

CHART 3: Previously Studied Perylene−Porphyrin Dyads and Benchmark Porphyrins

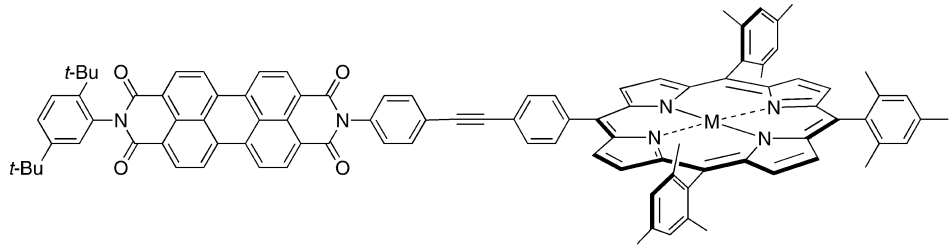

PDI-pep-Zn (M = Zn)
PDI-pep-Mg (M = Mg)
PDI-pep-Fb (M = H,H)

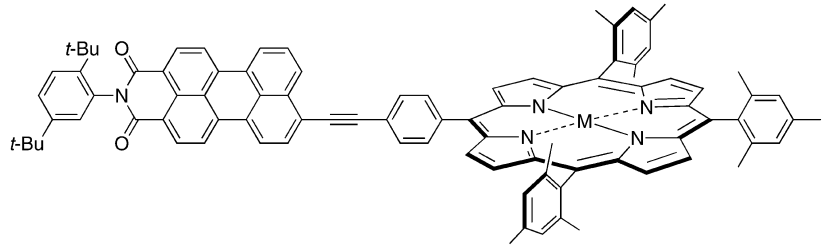

PMI-ep-Zn (M = Zn)
PMI-ep-Mg (M = Mg)
PMI-ep-Fb (M = H,H)

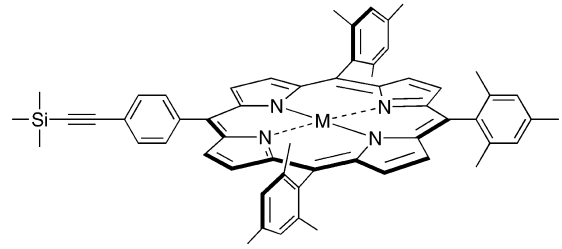

ZnU (M = Zn)
FbU (M = H,H)

perylene via a diphenylethyne (pep) linker. The second motif utilizes a perylene-monoimide (PMI) joined to the porphyrin at the C9 position of the perylene via an ethynylphenyl (ep) linker.[25] In both cases, the porphyrin is the free base (Fb), magnesium chelate (Mg), or zinc chelate (Zn).[27] The excited-state photochemical properties of these dyads are illustrated via consideration of the zinc chelates **PMI-ep-Zn** and **PDI-pep-Zn**. **PMI-ep-Zn** in toluene undergoes ultrafast (<0.5 ps) perylene-to-porphyrin energy transfer, followed by decay of the excited porphyrin as in the isolated pigment.[27] In acetonitrile, ultrafast electron transfer and charge recombination dominate the photochemical behavior.[29] The ultrafast dynamics are derived from the strong through-bond (linker-mediated) perylene−porphyrin electronic coupling indicated by the progressive red shift of the ground-state absorption of the perylene-monoimide (505 nm; **PMI-1**; Chart 1) upon successive addition of the ethyne (517 nm; **PMI-e**; Chart 1), phenyl (530 nm; **PMI-ep**; Chart 1), and porphyrin (548 nm; **PMI-ep-Zn**; Chart 3).[27] In comparison, **PDI-pep-Zn** in toluene or acetonitrile exhibits somewhat slower but still rapid (∼2.5 ps) parallel energy transfer (70−80%) and hole transfer (20−30%) from the photoexcited perylene to the porphyrin.[25,26] The excited porphyrin then decays (τ ∼4 ns) by electron transfer to the perylene. The lifetime of the charge-separated product varies from <0.5 ns to >10 ns depending on solvent polarity.

In this paper, we present the photophysical and redox properties of seven additional dyads containing a porphyrin and a perylene-monoimide. The dyads employ the best design features identified during studies of prior dyads. Thus, the perylene in each dyad is a monoimide derivative, the linker is attached to the *N*-imide or C9 position, and zero to three 4-*tert*-butylphenoxy groups (hereafter referred to as aryloxy groups) are incorporated for tailoring solubility and possible alteration of the electrochemical potentials. These dyads were designed to address two questions. To address the important question concerning the type of perylene-monoimide suitable for light-harvesting applications, four dyads were prepared each with a different perylene joined at the *p*-aryl position of a zinc porphyrin (Chart 4). A second question concerns the three-dimensional architecture of the dyad construct. To address this question, the perylene-monoimide found to be most suitable at the *p*-aryl position of the porphyrin was employed in dyads that utilized the *m*- or *o*-aryl position of a zinc porphyrin (Chart 5). One free base porphyrin also was prepared to explore possible mitigation of competing electron-transfer quenching processes. All of the dyads were examined by electrochemistry and static and time-resolved optical spectroscopy. Density functional theory (DFT) calculations were also performed on the various perylene-monoimides to examine the characteristics of the frontier molecular orbitals. Collectively, these studies identified suitable perylene−porphyrin motifs for use in multipigment light-harvesting arrays in polar and nonpolar media.

II. Experimental Section

A. Literature Compounds. Five of the seven perylene−porphyrin dyads[32] (***p*-PMI-aep-Zn**, ***p*-PMI(OR)-aep-Zn**, ***p*-PMI-(OR)$_3$-aep-Zn**, ***o*-PMI(OR)-aep-Zn**, and ***m*-PMI(OR)-aep-Zn**), all but one of the perylene benchmarks (**PMI-2**,[14,36] **PMI(OR)**,[32]

CHART 4: Dyads with Distinct Perylene-monoimides and a Common Porphyrin

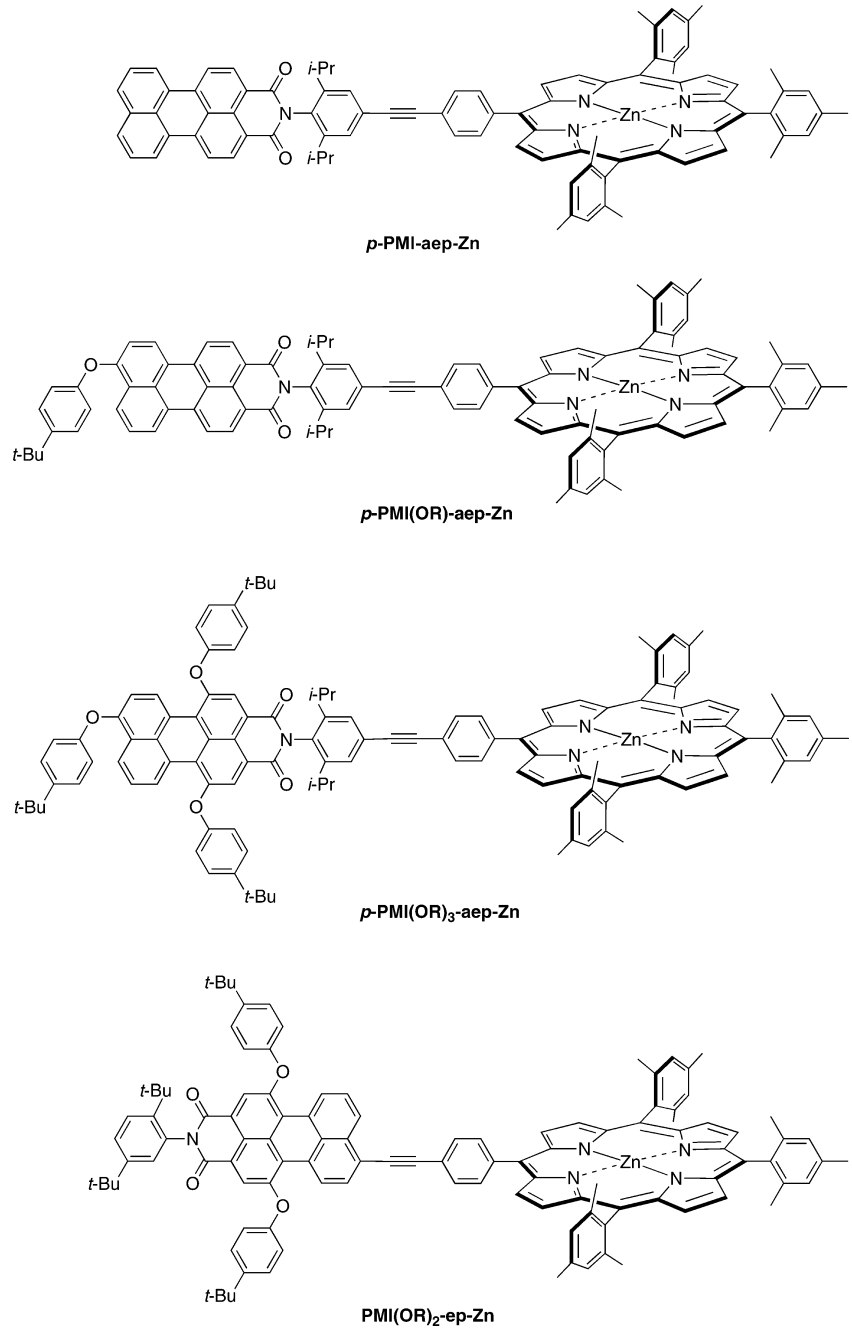

PMI(OR)-e,[32] **PMI(OR)$_3$-e**,[32,35] **PMI(OR)$_3$**,[35] and **PMI(OR)$_3$-1**[35]), and the porphyrin benchmarks (**ZnU**,[37] **FbU**[38]) were synthesized as described previously.

B. Synthesis. Three new compounds were prepared for the work described herein. Perylene building block[17] **PMI(OR)$_2$-Br** was treated with (trimethylsilyl)acetylene under Pd-catalyzed cross-coupling conditions with copper cocatalysis to afford the perylene benchmark **PMI(OR)$_2$-e-TMS** in 99% yield (Scheme 1). Analogous reaction of **PMI(OR)$_2$-Br** and the porphyrin building block 5,10,15-trimesityl-20-(4-ethynylphenyl)porphyrin (**ZnU′**)[39] under copper-free[39] Pd-catalyzed cross-coupling conditions gave the ethynylphenyl-linked perylene−porphyrin dyad **PMI(OR)$_2$-ep-Zn** in 60% yield. The dyad containing a free base porphyrin (***o*-PMI(OR)-aep-Fb**) was synthesized by demetalation of the corresponding zinc porphyrin construct upon treatment with trifluoroacetic acid in chloroform at room temperature.

1,6-Bis(4-tert-butylphenoxy)-9-[2-(trimethylsilyl)ethynyl]-N-(2,5-di-tert-butylphenyl)-3,4-perylenedicarboximide [PMI(OR)$_2$-e-TMS]. A mixture of **PMI(OR)$_2$-Br** (150 mg, 170 μmol), $Pd_2(dba)_3$ (7.8 mg, 8.5 μmol), PPh_3 (13.3 mg, 50.9 μmol), and CuI (3.2 mg, 17 μmol) in toluene/triethylamine [6 mL, (5:1)] was placed into an oil bath at 60 °C, and (trimethylsilyl)acetylene (28.7 μL, 203 μmol) was added. The mixture was stirred for 2.5 h and then passed over a silica column (4 × 25 cm, $CHCl_3$) to afford a red solid (152 mg, 99%): mp >300 °C; ^{1}H NMR (300 MHz, $CDCl_3$) δ 0.35 (s, 9H), 1.24 (s, 9H), 1.28 (s, 9H), 1.329 (s, 9H), 1.332 (s, 9H), 6.93 (d, 1H) [splittings are due to regioisomers], 7.04−7.09 (m, 4H), 7.39−7.43 (m, 5H), 7.53 (d, J = 8.4 Hz, 1H), 7.68 (t, J = 7.8 Hz, 1H), 7.77 (d, J = 8.1 Hz, 1H), 8.28 (d, J = 3.3 Hz, 2H), 8.46 (d, J = 7.5 Hz, 1H), 9.28 (d, J = 8.1 Hz, 1H), 9.40 (d, J = 6.9 Hz, 1H); FAB-

CHART 5: Dyads for Comparison of Architectural Distinctions and Energetic Differences

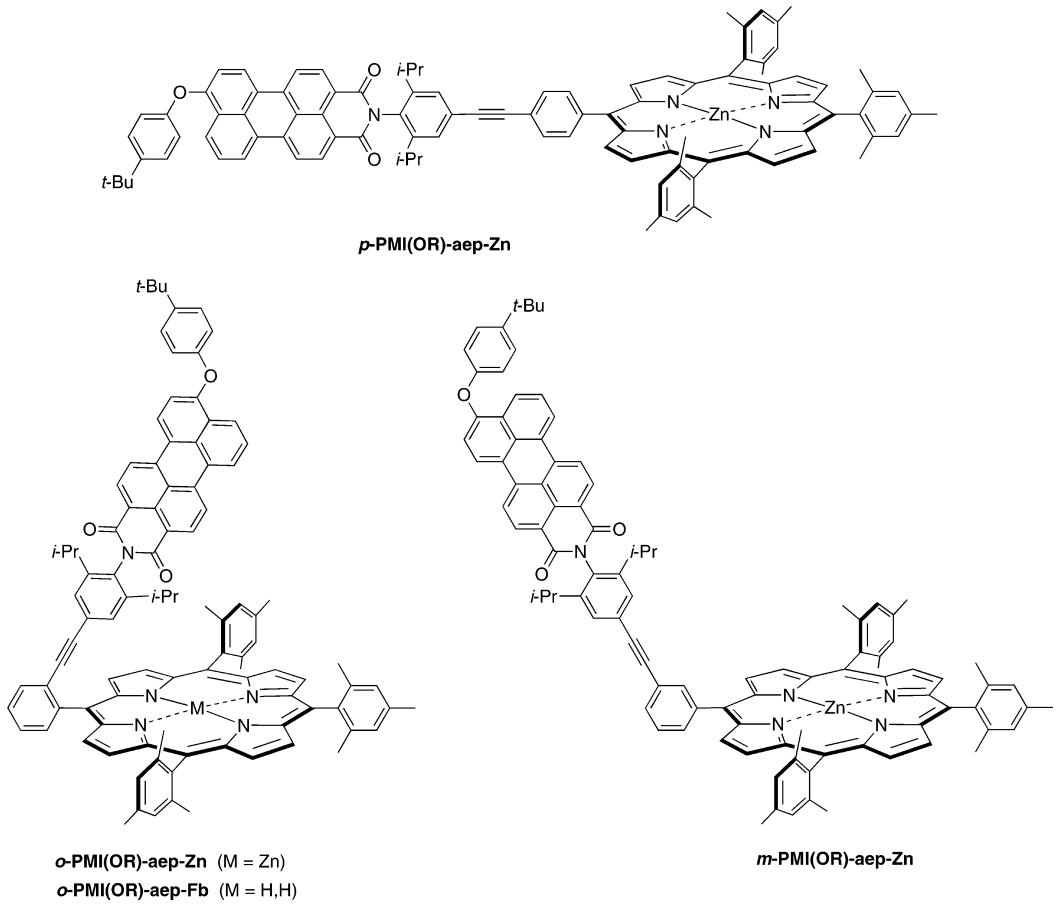

MS obsd 901.4571, calcd 901.4526 ($C_{61}H_{63}NO_4Si$); λ_{abs} (log ε) 421 (3.8), 487 (4.4), 520 (4.6) nm; λ_{em} (λ_{ex} = 520 nm) 551, 587(sh) nm.

9-[2-(4-(5,10,15-Trimesitylporphinatozinc(II)-20-yl)phenyl)-ethynyl]-1,6-bis(4-tert-butylphenoxy)-N-(2,5-di-tert-butylphenyl)-3,4-perylenedicarboximide [PMI(OR)$_2$-ep-Zn]. Following a standard procedure for copper-free Sonogashira coupling,[39] samples of 5,10,15-trimesityl-20-(4-ethynylphenyl)porphinatozinc(II) (**ZnU′**, 20.0 mg, 24.2 μmol) and **PMI(OR)$_2$-Br** (21.4 mg, 24.2 μmol) were coupled using $Pd_2(dba)_3$ (3.3 mg, 3.6 μmol) and P(*o*-tol)$_3$ (8.8 mg, 29 μmol) in degassed toluene/triethylamine [9.6 mL (5:1)] at 60 °C for 2 h. The reaction mixture was then concentrated and passed over a silica column [CH_2Cl_2/hexanes (1:1)]. Preparative SEC (THF) followed by column chromatography [silica, CH_2Cl_2/hexanes (2:1)] afforded a purple solid (23.6 mg, 60%): ^{1}H NMR (300 MHz, $CDCl_3$) δ 1.28 (s, 9H), 1.30 (s, 9H), 1.35 (s, 9H), 1.36 (s, 9H), 1.85 (s, 18H), 2.63 (s, 9H), 6.96 (d, J = 8.4 Hz, 1H), 7.11−7.15 (m, 4H), 7.28 (s, 6H), 7.41−7.47 (m, 5H), 7.55 (d, J = 8.4 Hz, 1H), 7.81 (t, J = 8.1 Hz, 1H), 7.99 (d, J = 8.1 Hz, 1H), 8.05 (d, J = 8.1 Hz, 2H), 8.29 (d, J = 8.1 Hz, 2H), 8.34 (s, 2H), 8.69−8.91 (m, 9H), 9.43 (d, J = 8.1 Hz, 1H), 9.49 (d, J = 7.5 Hz, 1H); LD-MS obsd 1633.09; calcd average mass 1632.40 ($C_{111}H_{99}N_5O_4Zn$); λ_{abs} 424, 549, 591 nm; λ_{em} (λ_{ex} = 550 nm) 599, 646 nm.

5-[2-(2-(4-(9-(4-tert-Butylphenoxy)-3,4-perylenedicarboximido)-3,5-diisopropylphenyl)ethynyl)phenyl]-10,15,20-trimesitylporphyrin [o-PMI(OR)-aep-Fb]. A sample of ***o*-PMI(OR)-aep-Zn** (10.5 mg, 7.21 μmol) in $CHCl_3$ (10 mL) at room temperature was treated with TFA (8.3 mL, 110 μmol). After stirring for 15 min, TEA (200 μL) was added. The mixture was passed through a silica column ($CHCl_3$, 3 × 10 cm) to afford a magenta solid (9.1 mg, 91%): ^{1}H NMR (400 MHz, $CDCl_3$) δ −1.64 (s, 2H), −0.21 (dd, J^1 = 6.4 Hz, J^2 = 1.2 Hz, 12H), 1.36 (s, 9H), 1.80 (s, 3H), 1.82 (s, 6H), 1.84 (s, 6H), 1.86 (s, 3H), 1.90 (m, 2H), 2.58 (s, 3H), 2.62 (s, 6H), 5.51 (s, 2H), 6.87 (d, J = 8.4 Hz, 1H), 7.07 (d, J = 8.4 Hz, 2H), 7.20 (s, 1H), 7.25 (brs, 5H), 7.43 (d, J = 8.8 Hz, 2H), 7.57 (t, J = 7.6 Hz, 1H), 7.70 (t, J = 7.2 Hz, 1H), 7.80 (t, J = 8.0 Hz, 1H), 8.01 (d, J = 7.2 Hz, 1H), 8.07 (d, J = 8.4 Hz, 1H), 8.14 (d, J = 6.8 Hz, 1H), 8.19 (d, J = 8.8 Hz, 1H), 8.23−8.32 (m, 3H), 8.35 (d, J = 8.4 Hz, 1H), 8.38 (d, J = 7.6 Hz, 1H), 8.56−8.59 (m, 4H), 8.67 (d, J = 4.4 Hz, 2H), 8.74 (d, J = 4.4 Hz, 2H); LD-MS obsd 1391.0, calcd average mass 1392.77 ($C_{99}H_{85}N_5O_3$); λ_{abs} 420, 485, 513, 593, 649 nm; λ_{em} (λ_{ex} = 513 nm) 649, 719 nm.

C. Electrochemistry. The electrochemical studies were performed in butyronitrile (Burdick and Jackson) using previously described instrumentation.[40] The supporting electrolyte was 0.1 M tetrabutylammonium hexafluorophosphate (Aldrich; recrystallized three times from methanol and dried at 110 °C in vacuo). The electrochemical cell was housed in a Vacuum Atmospheres glovebox (model HE-93) equipped with a Dri-Train (model 493). The $E_{1/2}$ values were obtained with square wave voltammetry (frequency 10 Hz).

D. Spectroscopy and Analysis. The transient-absorption measurements were conducted on the arrays in toluene or benzonitrile (PhCN) at 295 K (5−30 μM solutions in 2 mm path cells). These measurements employed ∼130 fs, 25−30 μJ, excitation flashes (focused to ∼1 mm diameter) at 490 nm and white-light probe pulses of comparable duration.[27] The excitation flashes were attenuated to ∼8 μJ to avoid exciton annihilation,[41,42]

SCHEME 1: Synthesis of Perylene−Porphyrin Dyad PMI(OR)$_2$-ep-Zn and Control Monomer PMI(OR)$_2$-e-TMS

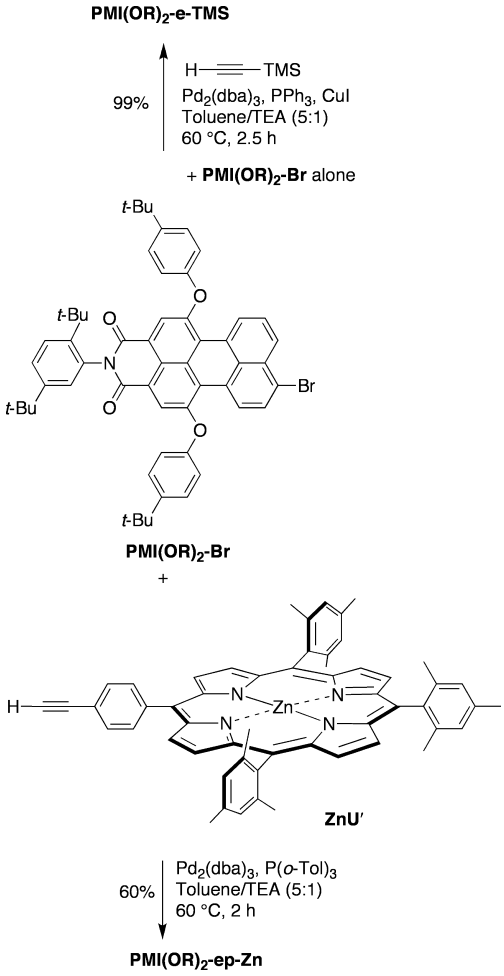

which if present adds a short 1−3 ps component to the photodynamics. For each dyad and solvent, a data set was obtained that encompassed wavelengths 505−750 nm and times from −20 ps to 3.9 ns. Global analysis of the transient-absorption data for a given array was performed using IgorPro6 (Wavemetrics) for data sets in which ΔA in each spectrum was averaged in 5 nm steps across the range 505−680 nm. The resulting kinetic traces for pump−probe delay times from −20 to 200 ps or 3.9 ns (depending on sample) were globally fit using the convolution of the instrument response with function consisting of one or more exponentials plus a constant. Some curve fitting of individual kinetic traces utilized Origin8 (Microcal).

E. Molecular Orbital Calculations. Density-functional-theory (DFT) calculations were performed with Spartan '06 for Windows (Wave function, Inc.) on a PC (Dell Optiplex GX270) equipped with a 3.2 GHz CPU and 3 GB of RAM.[43] The hybrid B3LYP functional and a 6-31G* basis set were employed. The equilibrium geometries were fully optimized using the default parameters of the Spartan '06 program. The TMS group of **PMI(OR)$_2$-e-TMS** was replaced with H to simplify the calculations.

III. Results

A. Electrochemical Characteristics. The electrochemical data for the benchmark perylene-monoimides are summarized in Table 1. The data for the perylene−porphyrin dyads are given in Table 2. The data in Table 1 focus on the two reduction waves of the perylene, the first being in the range from −1.1 to −1.3 V and the second typically being in the range from −1.6 to −1.8 V. The first and second oxidation waves for the two perylene monomers bearing three aryloxy groups were also measured and were found to be about +0.8 and +1.2 V (see Table 1 footnotes). These results are consistent with our previous studies of related perylene compounds.[25,27]

The redox characteristics of the perylene units in the dyads are essentially identical to those of the isolated chromophores. In all cases, the $E_{1/2}$ values of the perylenes in the dyads are within a few mV of those of the benchmarks. The zinc porphyrin unit in each dyad exhibits two oxidation waves and two reduction waves in the +1.0 to −2.0 V range; the oxidation potentials are listed in Table 2 because they are most relevant to the studies herein. The $E_{1/2}$ values for zinc porphyrins are similar among the dyads and essentially identical to those of structurally related tetraarylporphyrin monomers.[44] These data are indicative of relatively weak ground-state electronic interactions between the perylene and porphyrin constituents of the dyad.

TABLE 1: Half-Wave Potentials and Molecular-Orbital Energies for Perylene Monomers[a]

	reduction potentials		molecular-orbital energies	
perylene monomer	$E_{1/2}$ (1) (V)	$E_{1/2}$ (2) (V)	HOMO (eV)	LUMO (eV)
PMI-1	−1.24[b]	−1.79[b]	−5.52	−2.78
PMI-e	−1.16[b]	−1.65[b]	−5.53	−2.92
PMI-2	−1.21	−1.81	−5.54	−2.81
PMI(OR)	−1.21	−1.78	−5.31	−2.67
PMI(OR)$_2$-e-TMS	−1.13	−1.61	−5.23	−2.68
PMI(OR)$_3$	−1.32	−1.78	−5.04	−2.47
PMI(OR)$_3$-e	−1.30	−1.77	−5.10	−2.54

[a] Obtained in butyronitrile containing 0.1 M TBAH. $E_{1/2}$ vs Ag/Ag$^+$; $E_{1/2}$ of $FeCp_2/FeCp_2^+$ = +0.19 V. (Add +0.26 V to obtain the values versus SCE.) The $E_{1/2}$ values are obtained from square wave voltammetry (frequency = 10 Hz). Values are ±0.01 V. The first and second oxidation potentials were also measured for **PMI(OR)$_3$** and are +0.81 and +1.19 eV, respectively. Essentially the same values were found for **PMI(OR)$_3$-e** (+0.82 and +1.19 eV). [b] From ref 27.

TABLE 2: Half-Wave Potentials ($E_{1/2}$) for the Perylene−Porphyrin Dyads[a]

	porphyrin oxidation potentials[b]		perylene reduction potentials	
dyad	$E_{1/2}$ (1) (V)	$E_{1/2}$ (2) (V)	$E_{1/2}$ (1) (V)	$E_{1/2}$ (2) (V)
PMI-ep-Zn[c]	+0.50	+0.88	−1.14	−1.60
***p*-PMI-aep-Zn**	+0.52	+1.08	−1.19	−1.81[d]
***p*-PMI(OR)-aep-Zn**	+0.52	+0.96	−1.19	−1.73[d]
***m*-PMI(OR)-aep-Zn**	+0.52	+0.96	−1.19	−1.73[d]
***o*-PMI(OR)-aep-Zn**	+0.51	+0.96	−1.20	−1.76[d]
PMI(OR)$_2$-ep-Zn	+0.52	+0.96	−1.13	−1.57
***p*-PMI(OR)$_3$-aep-Zn**	+0.52	+0.92	−1.30	−1.76[d]

[a] Obtained in butyronitrile containing 0.1 M TBAH. $E_{1/2}$ vs Ag/Ag$^+$; $E_{1/2}$ of $FeCp_2/FeCp_2^+$ = +0.19 V. (Add +0.26 V to obtain the values versus SCE.) The $E_{1/2}$ values are obtained from square wave voltammetry (frequency = 10 Hz). Values are ±0.01 V. [b] The potential is approximate because the second oxidation wave of the porphyrin partially overlaps the first oxidation wave of the perylene. The second perylene oxidation potential was measured for ***p*-PMI(OR)$_3$-aep-Zn** (+1.19 V). [c] Taken from ref 27. [d] The potential is approximate because the second reduction wave of the perylene strongly overlaps the first reduction wave of the perylene.

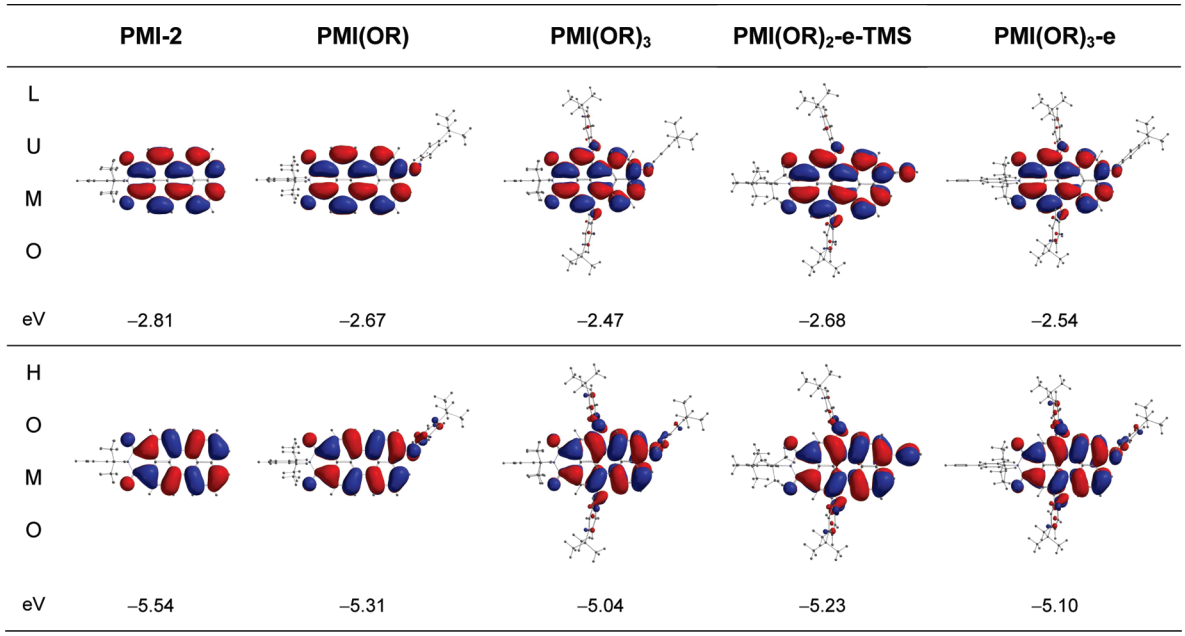

Figure 1. Electron density distributions and energies for the frontier molecular orbitals of perylene monomers, obtained from DFT calculations.

One particularly noteworthy feature of the redox properties of the perylene compounds is that the addition of one aryloxy group has a minimal effect, and up to three aryloxy groups only a modest effect, on the redox potentials. For example, the first reduction potentials for **PMI-2**, **PMI(OR)**, and **PMI(OR)$_3$** are −1.21, −1.21, and −1.32 V, respectively. A similar trend is observed for the second reduction potentials and for the set **PMI-e**, **PMI(OR)$_2$-e-TMS**, and **PMI(OR)$_3$-e** (Table 1). Likewise, for the dyads, the perylene first reduction potentials for ***p*-PMI-aep-Zn**, ***p*-PMI(OR)-aep-Zn**, and ***p*-PMI(OR)$_3$-aep-Zn** are −1.19, −1.19, and −1.30 V, respectively, and similarly for the second reduction potentials.

The observation that the addition of an alkoxy group to the C9 position of the perylene (**PMI(OR)** versus **PMI-2**) has very little effect on the redox potentials is surprising in view of the fact that the addition of an alkynyl group at this position (**PMI-e** versus **PMI-1**) shifts the reduction potentials positively by an average of 0.1 V (Table 1). Possibly, the electron-donating property of the alkoxy group is balanced by a nearly equal and opposite inductive effect. However, there is a small incremental effect when two additional aryloxy groups are added to the perylene 1- and 6-positions. On the basis of the first reduction potentials for the perylene monomers, the addition of three aryloxy groups makes the perylene harder to reduce by an average of 0.12 V. This prediction is realized in the dyads, wherein ***p*-PMI(OR)$_3$-aep-Zn** is harder to reduce than ***p*-PMI-aep-Zn** by 0.11 V. Thus, the addition of three aryloxy groups to the perylene to increase solubility has the added benefit of rendering the dyad slightly less susceptible to electron-transfer quenching. This is so because the lowest-energy electron-transfer process for a photoexcited perylene−porphyrin dyad will generally involve reduction of the perylene (and oxidation of the porphyrin) on the basis of the redox potentials given in Tables 1 and 2 and prior work.[25–27]

B. Molecular Orbital Characteristics. The molecular orbital characteristics (energies and electron-density distributions) for the benchmark perylenes were examined to gain further insights into the redox potentials (Figure 1). Paralleling the comparisons of reduction potentials given above, the LUMO energy for **PMI-2** is −2.81 eV, whereas that for **PMI(OR)** is −2.67 eV and that for **PMI(OR)$_3$** is −2.47 eV. A similar trend is observed for **PMI-e**, **PMI(OR)$_2$-e-TMS**, and **PMI(OR)$_3$-e**. A less negative reduction potential implies that the molecule is easier to reduce. Thus, although the directions of the shifts in orbital energies track the shifts of the reduction potentials, the effect of the aryloxy groups on the orbital energies is (about 3-fold) larger than that on the redox potentials. This difference likely arises in part from the effect of solvation to modulate the effects of the aryloxy groups on the redox potentials measured for the perylenes in solution compared to the orbital energies calculated for the same molecules in the gas phase.

C. Photophysical Properties of Perylene Benchmark Monomers. ***1. Absorption and Fluorescence Spectra, Fluorescence Yields, and Singlet Excited-State Lifetimes.*** The structures of perylene monomers investigated here are shown in Chart 2. The absorption spectra of the perylene-monoimide monomers bearing no aryloxy substituents (**PMI-2**), one aryloxy group [**PMI(OR)**], or three aryloxy groups [**PMI(OR)$_3$**] all display a broad absorption manifold (fwhm ∼75 nm) consisting of a series of substantially overlapping vibronic transitions. The presence of one or three aryloxy substituents results in a bathochromic shift of approximately 30 nm, such that the (0,0) band moves from 506 nm in **PMI-2** to 532 nm in **PMI(OR)**, 532 nm in **PMI(OR)$_3$**, and 536 nm in **PMI(OR)$_3$-e** in toluene. A similar trend is observed for the same compounds in PhCN except that in each case there is a 3−10 nm red-shift compared to that in toluene. For benchmark perylenes having an ethyne directly attached to the perylene C9 position, the (0,0) band moves from 505 nm in **PMI-1** to 517 nm in **PMI-e** (Chart 1) as found previously,[27] to 527 nm for **PMI(OR)$_2$-e-TMS** (Chart 2). Collectively, these observations indicate that the dominant contribution to the spectral shift stems from substitution at the 9-position of the perylene; further substitution of two aryloxy groups at the flanking positions (1-, 6-) of the perylene or incorporation of the ethyne group on the aryl ring at the *N*-imide position generally has a more modest effect on the spectral properties.

Each of the perylene-monoimide monomers has a broad fluorescence contour that is approximately a mirror image to the absorption manifold. In analogy to the absorption spectrum,

TABLE 3: Photophysical Properties of Perylene−Porphyrin Dyads and Reference Monomers[a]

	toluene		PhCN	
	Φ_f	τ_S (ns)	Φ_f	τ_S (ns)
	Dyads			
***p*-PMI-aep-Zn**	0.042	2.4	0.040	2.0
***p*-PMI(OR)-aep-Zn**	0.046	2.4	0.043	1.9
***p*-PMI(OR)$_3$-aep-Zn**	0.048	2.4	0.041	1.8
***o*-PMI(OR)-aep-Zn**	0.036	2.4	0.023	1.4
***m*-PMI(OR)-aep-Zn**	0.038	2.4	0.041	2.1
***o*-PMI(OR)-aep-Fb**	0.082	13.6	0.085	13.3
PMI(OR)$_2$-ep-Zn	0.070	2.4	≤0.003	0.005
	Monomers			
PMI-2	0.91[b]	5.0[b]	0.99	5.2
PMI(OR)	0.82[b]	4.8[b]	0.79	4.8
PMI(OR)$_3$-e	0.86[b]	5.0[b]	0.92	5.2
PMI(OR)$_3$	0.97	5.3	0.96	5.2
PMI(OR)-e	0.72	5.0	0.74	4.6
PMI(OR)$_2$-e-TMS	0.90	5.0	0.97	5.0
PMI(OR)$_3$-1	0.85	5.5	0.90	5.4
ZnU	0.034[b]	2.4[b]	0.041	2.0[b]
FbU	0.090	13.3[c]	0.096	13.3

[a] All data at room temperature in Ar-purged (deaerated) solution. [b] From ref 30. [c] From ref 46.

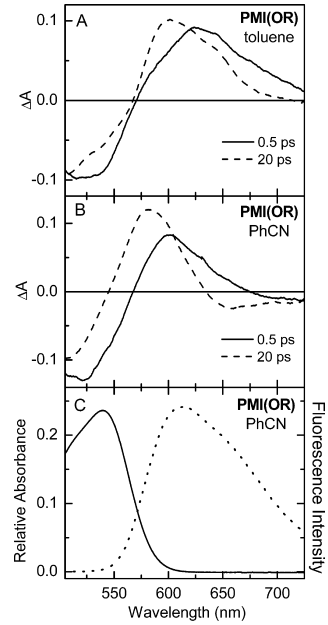

Figure 2. Time-resolved absorption difference spectra at 0.5 ps (solid) and 20 ps (dashed) after excitation with a 130 fs 490 nm excitation flash for **PMI(OR)** in toluene (A) and PhCN (B). Ground-state absorption (solid) and fluorescence (dotted) features for **PMI(OR)** in PhCN are given for comparison (C).

the fluorescence spectrum red-shifts upon incorporation of the aryloxy substituents. On the other hand, the presence of aryloxy groups does not significantly affect the fluorescence quantum yield of the perylene-monoimide (Table 3). The high (>0.7) fluorescence yields of the perylene-monoimide monomers both in toluene and PhCN indicate that the excited singlet state of each of these chromophores has only minor nonradiative decay competing with the fluorescence emission process. These perylene monomers also have long (∼5 ns) fluorescence lifetimes (Table 3). Similar properties have been reported for other perylene-monoimides.[26,27,30,45] The spectroscopic properties of the porphyrin benchmarks **ZnU** and **FbU** have been examined previously[30,46] and are included in the table for comparison.

2. Time-Resolved Absorption Spectra and Excited-State Relaxation Dynamics. Transient absorption spectra were acquired for perylene-monoimide monomers (bearing zero, one, or three aryloxy substituents) in toluene and in PhCN utilizing 130 fs excitation flashes at 490 nm and a time delay of 3.5 ns. Representative spectra for **PMI(OR)** in toluene and in PhCN are given in parts A and B of Figure 2, respectively. For comparison, ground-state absorption spectra (solid) and fluorescence spectra (dotted) are given in Figure 2C. The absorption difference spectrum for **PMI(OR)** in PhCN at 0.5 ps includes bleaching of the broad ground-state absorption band at ∼530 nm (Figure 2B). This negative-going contribution is overlapped with singlet-excited-state stimulated emission (fluorescence stimulated by the white-light probe pulse) that also gives a negative-going contribution to the difference spectrum. The 0.5 ps spectrum also shows a broad excited-state absorption (positive-going contribution) at wavelengths >570 nm.

At 20 ps, there is an overall diminution of the combined bleaching plus stimulated-emission feature between 510 and 570 nm, giving way to increased net excited-state absorption in this region. In contrast, there is a net decrease in the excited-state absorption at wavelengths >570 nm. This latter characteristic is due at least in part to the growth of stimulated emission in this region that is expected to have the general profile of steady-state spontaneous fluorescence (Figure 2C, dotted line). This combination results in a net negative-going feature between 650 and 730 nm in the 20 ps spectrum (Figure 2B, dashed line).

The spectrum at 20 ps then partially decays in a uniform manner (no change in shape) out to the 3.9 ns limit of the experiment and with a time constant of ∼5 ns (not shown). These findings on **PMI(OR)** in PhCN are consistent with (i) the 4.8 ns singlet excited-state lifetime derived from the fluorescence measurements (Table 3) and (ii) the decay of the perylene lowest singlet excited state being dominated by return to the ground state (largely by fluorescence) with little formation of a longer lived triplet excited state. A similar time evolution of the spectrum is observed for **PMI(OR)** in toluene (Figure 2A).

Representative kinetic profiles (555 and 665 nm) for the spectral evolution for **PMI(OR)** in PhCN are shown in Figure 3A. The solid lines are fits to convolution of the instrument response plus the single-exponential function $A\exp(-t/\tau) + C$. The globally fit time constant is 6.4 ps. Analogous spectral and kinetic data were acquired for the other perylene monomers in toluene and PhCN (see the Supporting Information). The time constants for the excited-state evolution for different perylene/solvent combinations are in the range 3.2−6.6 ps (Table 4).

The simplest interpretation of the spectral time evolution in each case is as follows. The spectra at 0.5 ps for each perylene-monoimide monomer are assigned to the initial Franck−Condon form of the singlet excited state (denoted PMI**; formed by single-photon absorption and not a two-photon process). This initial excited-state form may differ conformationally, vibrationally, and/or electronically from the relaxed, lowest-energy singlet excited-state form (denoted PMI*). State PMI* for each perylene is responsible for the observed spontaneous fluorescence spectrum and the fluorescence quantum yield and singlet-excited-state lifetime listed in Table 3. The stimulated emission (and presumably spontaneous fluorescence) from PMI** occurs at shorter wavelengths than that from PMI*.

Thus, the time evolution of the spectrum that occurs for each perylene-monoimide during the first 10 ps after excitation reflects a "dynamic Stokes shift". This evolution likely involves a change in internal coordinates (conformational/vibrational/

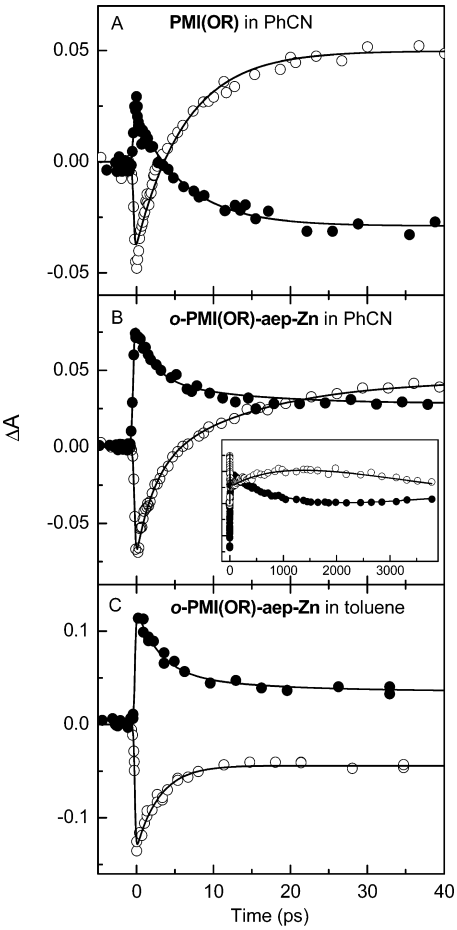

Figure 3. Representative kinetic profiles for (A) perylene monomer **PMI(OR)** in PhCN at 555 nm (open circles) and 665 nm (closed circles), (B) perylene−porphyrin dyad ***o*-PMI(OR)-aep-Zn** in PhCN at 520 nm (open circles) and 616 nm (closed circles), and (C) ***o*-PMI(OR)-aep-Zn** in toluene at 545 nm (open circles) and 660 nm (closed circles) obtained using 130 fs excitation flashes at 490 nm. The inset in panel B shows the data on an expanded time scale. The solid lines are fits to a function consisting of the instrument response convolved with one (A), two (C), or four (B) exponentials plus a constant.

TABLE 4: Rate Constants for Fast Relaxation in Perylene Monomers

	$(k_{rel})^{-1}$ (ps)	
perylene monomer	toluene	PhCN
PMI-2	3.2	6.6
PMI(OR)	5.3	6.4
PMI(OR)$_3$-e	5.1	6.0
PMI(OR)$_3$	4.8	6.5

electronic) of the perylene as well as a change in the interaction of the perylene with the medium. The dependence of the relaxation rate (Table 4) and the associated evolution of the spectra in Figure 2 suggest that the process depends on the presence and number of the aryloxy groups. The nature of the relaxation process may have some analogies to the dynamics that we have described previously for difluoroboron-dipyrrin[47,48] and bis(dipyrrinato)zinc(II)[49] chromophores. For those two classes, following excitation, there is a picosecond time scale relaxation to a lower energy excited-state form involving changes in the structure and electronic character of the chromophore. For the perylenes studied here, the dynamics may be in part connected with internal rotation of the aryloxy groups with respect to the perylene core along with distortions of the latter. Such motions in turn would modulate the electron distribution involving the perylene and aryloxy groups and thus the relative extent of charge-transfer character in PMI* compared to PMI** and compared to the ground electronic state. Differences in charge-transfer character between the two excited-state forms would also cause a change in the interactions of the perylene with the solvent. Whatever the origin, the presence of two excited-state forms for the PMI has consequences for the energy-transfer dynamics in the dyads, as described below.

3. The Effect of Solvent on the Optical Properties. To further probe the issues raised above concerning the excited-state dynamics of the perylenes, the absorption and fluorescence spectra of **PMI-2**, **PMI(OR)**, and **PMI(OR)$_3$-e** were measured in a range of solvents having different refractive indices (n) and dielectric constants (ε). These values for each solvent and the spectra are given in the Supporting Information. As noted above, the spectra are characterized by an intense band in the 400−600 nm region. Vibronic structure is typically resolved in nonpolar solvents such as hexane but not in polar solvents such as methanol. Figure 4A,C,E shows plots of the wavenumber position of the absorbance maximum as a function of solvent polarizability, $R(n) = (n^2 - 1)/(n^2 + 2)$. There is a good linear correlation between this function and peak position for samples in nonpolar solvents but not in polar media. The same is true for the peak position of the fluorescence (Figure 4G,I,K). Figure 4B,D,F shows that the peak absorption position also varies with solvent polarity, $P(\varepsilon) = (\varepsilon - 1)/(\varepsilon + 2)$. This relationship is linear for the samples in nonpolar solvents, and the same is true except for **PMI(OR)$_3$-e** in polar solvents. Figure 4H,J,L shows similar plots for the emission position. In this case, a linear relationship is observed for all three compounds in both polar and nonpolar media. In terms of both the dielectric constant and the index of refraction of the solvent, the shifts are more pronounced for fluorescence than for absorbance position. The solvent dependence of the optical properties depicted in Figure 4 may be due to dispersive interactions between the solvent and the perylene. The collective data suggest that the excited state (PMI**, PMI*, or both) has a larger dipole moment than the ground state.[50]

D. Photophysical Properties of Diarylethyne-Linked Perylene−Porphyrin Dyads. ***1. Absorption and Fluorescence Spectra, Fluorescence Yields, and Singlet Excited-State Lifetimes.*** Figure 5 shows ground-state absorption spectra of perylene−porphyrin dyad ***p*-PMI-aep-Zn** and reference compounds **PMI-2** and **ZnU** in toluene (solid lines). The spectrum of the dyad closely matches the sum of the spectra of the component parts. This comparison indicates that the perylene−porphyrin electronic interactions in the ground and lowest singlet excited state are weak (but not necessarily insignificant). This conclusion is consistent with that drawn above about the ground-state perylene−porphyrin interactions on the basis of the redox data. The same conclusions are drawn from the optical and redox data for all of the perylene−porphyrin arrays that employ the diarylethyne (-aep-) linker (Chart 4).

The fluorescence spectra of dyad ***p*-PMI-aep-Zn** and reference monomers **PMI-2** and **ZnU** in toluene are also shown in Figure 5 (dashed lines). The emission of ***p*-PMI-aep-Zn** was measured using excitation at several wavelengths at which either the perylene or the porphyrin primarily absorbs. Upon illumination of ***p*-PMI-aep-Zn** in toluene in 490 nm, where the perylene absorption is >100-fold that of the porphyrin, the emission is dominated by fluorescence from the porphyrin (Figure 5A, dashed spectrum). This finding is consistent with substantial energy transfer from the photoexcited perylene (PMI* and

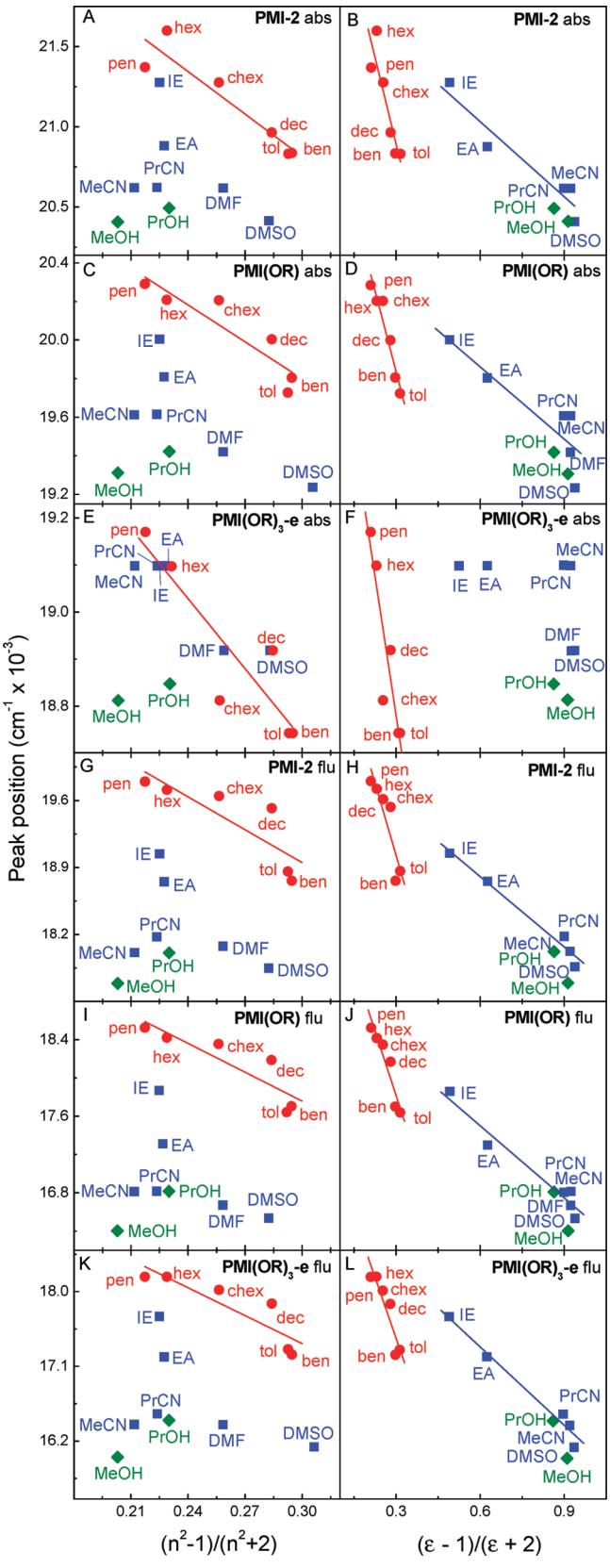

Figure 4. Peak positions of the ground state absorption maxima (A−F) and fluorescence maxima (G−L) for perylene monomers as a function of the solvent polarizability (left panels) and polarity (right panels). Solvent abbreviations: ben = benzene, chex = cyclohexane, dec = decalin, DMF = dimethylformamide, DMSO = dimethylsulfoxide, EA = ethyl acetate, hex = hexane, IE = isopropyl ether, MeCN = acetonitrile, MeOH = methanol, pen = isopentane, PrCN = propionitrile, PrOH = 2-propanol, tol = toluene.

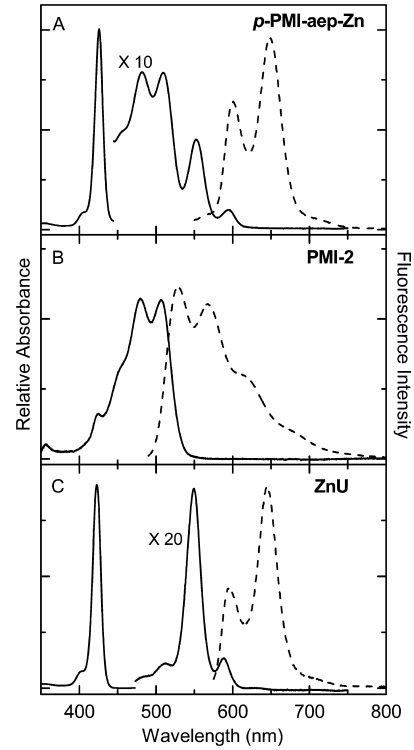

Figure 5. Ground-state absorption spectra (solid) and fluorescence spectra (dashed) of diarylethyne-linked perylene−porphyrin dyad (A), benchmark perylene (B), and benchmark porphyrin (C) in toluene.

PMI** as discussed below) to the ground-state zinc porphyrin to produce the porphyrin lowest singlet excited state (Zn*). The dyad was also illuminated at 560 nm where the zinc porphyrin is primarily excited. As expected, emission occurs essentially exclusively from the porphyrin.

The fluorescence quantum yield (Φ_f ~0.04) for ***p*-PMI-aep-Zn** is essentially the same (i) using excitation of the perylene or the porphyrin, (ii) for the dyad in toluene or PhCN, and (iii) as reference monomer **ZnU** (Table 3). Similarly, the singlet excited-state lifetime (τ_S) of ***p*-PMI-aep-Zn** in toluene or PhCN is the same as that for **ZnU** in toluene (2.4 ns) or PhCN (2.0 ns). These data indicate that (i) energy transfer from perylene to porphyrin is basically quantitative and (ii) there is no appreciable quenching of the Zn* due to the presence of the perylene (or of PMI* due to the porphyrin), even in polar media.

Inspection of Table 3 indicates that similar conclusions can be drawn concerning quantitative perylene to porphyrin energy transfer without any significant electron-transfer quenching (of either the excited perylene or excited porphyrin) for dyads ***p*-PMI(OR)-aep-Zn** and ***m*-PMI(OR)-aep-Zn** in toluene or PhCN, and for dyads ***p*-PMI(OR)$_3$-aep-Zn** and ***o*-PMI(OR)-aep-Zn** in toluene. In the case of ***p*-PMI(OR)$_3$-aep-Zn** in PhCN, there is a hint of excited-state quenching (≤10%) based on a slightly diminished porphyrin τ_S value of 1.8 ns compared to 2.0 ns for **ZnU** in PhCN; however, because this difference is at the margins of the ±0.1 ns error in these values, the quenching is not significant if it does occur.

The exception to the behavior described above is for dyad ***o*-PMI(OR)-aep-Zn** in PhCN. Although the fluorescence yield is again about the same for excitation of perylene or porphyrin (indicative of quantitative energy transfer to the porphyrin), in both cases, the Φ_f value (0.023) is lower than that for **ZnU** in this medium (0.041). Similarly, the τ_S value for the dyad (1.4 ns) is smaller than that for **ZnU** (2.0 ns). These combined results reflect efficient perylene-to-porphyrin energy transfer but with

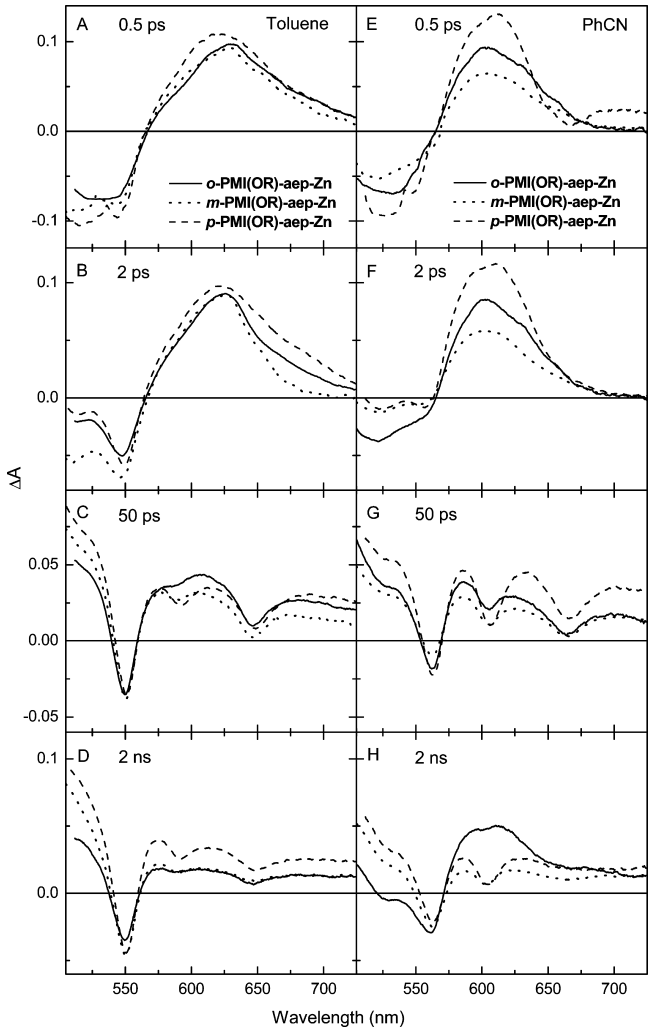

Figure 6. Time-resolved absorption difference spectra for perylene−porphyrin dyads in toluene and PhCN obtained using 130 fs 490 nm excitation flashes.

subsequent quenching of Zn* by the perylene. The fact that this quenching occurs in PhCN but not toluene suggests that electron transfer is the source of the quenching. The rate constant and yield (~30%) for this quenching process will be derived below.

When the zinc porphyrin of ***o*-PMI(OR)-aep-Zn** is replaced by the free base in analogue ***o*-PMI(OR)-aep-Fb**, no quenching is observed in either toluene or PhCN. Compared to zinc porphyrins, the free base porphyrins in the dyads have larger Φ_f values (0.09) and τ_S values (~13 ns) (Table 3), just like the **FbU** reference monomer, both in toluene and PhCN. These results are again indicative of quantitative perylene-to-porphyrin energy transfer with no indication of excited-state electron-transfer quenching in nonpolar and polar media.

2. Time-Resolved Absorption Spectra. Figure 6A−D shows representative time-resolved absorption spectra for the trio of architecturally distinct dyads ***o*-PMI(OR)-aep-Zn**, ***m*-PMI(OR)-aep-Zn**, and ***p*-PMI(OR)-aep-Zn** in toluene. In each case, the perylene was preferentially excited with a 130 fs flash at 490 nm. The same general behavior is observed in each case. The spectrum at 0.5 ps (Figure 6A) is basically identical to that for the benchmark perylene monomer **PMI(OR)** immediately after excitation (Figure 2A, solid line) and is thus attributed to the unrelaxed perylene singlet excited state PMI**. Modest changes in the spectra occur by 2 ps (Figure 6B) that reflect those seen for **PMI(OR)** at 20 ps and are attributed to the relaxed perylene singlet excited state PMI* (Figure 2A, dashed line). The 2 ps spectra for the dyads also show a small bleaching in the porphyrin Q(1,0) ground-state absorption band at 550 nm (see Figure 5C), indicating that some energy has moved from the perylene to the porphyrin. The porphyrin Q(1,0) bleaching at 550 nm is fully developed by 50 ps (Figure 6C), and is accompanied by the expected (see Figure 5C) small Q(0,0) bleaching plus stimulated emission at 585 nm and the pronounced Q(0,1) stimulated emission at 650 nm. All of these features indicate that the spectrum of each of the three dyads in toluene at 50 ps can be attributed to Zn*. These features have uniformly and partially decayed by 2 ns (Figure 6D) and further still by the 3.9 ns limit of the measurement.

The same behavior is also observed for toluene solutions of all the other dyads employing a diarylethyne linker attached at the *N*-imide position of the perylene: ***p*-PMI-aep-Zn**, ***p*-PMI-(OR)$_3$-aep-Zn**, and ***o*-PMI(OR)-aep-Fb**. The only differences among these cases are the detailed kinetics (described below) and differences in the porphyrin excited-state spectra at 50 ps. The latter reflect the changes in the positions of the ground-state absorption bands (and thus bleaching features in the transient spectra) and spontaneous fluorescence bands (and thus stimulated-emission features in the transient spectra) due to (i) the number of aryloxy groups on the perylene and (ii) the porphyrin being a zinc chelate (and formation of Zn*) or the free base (formation of Fb*).

Figure 6E−H shows representative time-resolved absorption spectra for the trio of architecturally distinct dyads ***o*-PMI(OR)-aep-Zn**, ***m*-PMI(OR)-aep-Zn**, and ***p*-PMI(OR)-aep-Zn** in PhCN. Similar data were also found for ***p*-PMI-aep-Zn**, ***p*-PMI(OR)$_3$-aep-Zn**, and ***o*-PMI(OR)-aep-Fb** in PhCN. In all six cases, the spectral evolution from 0.5 to 2 ps and then to 50 ps (Figure 6E−G) is similar to that described above for the dyads in toluene (Figure 6A−C). Again, the only differences for a particular compound in PhCN versus toluene are the detailed kinetic profiles and, for dyads containing a zinc porphyrin, the positions and relative intensities of the various bleaching and stimulated-emission features due to coordination of solvent molecules to the central zinc ion, as expected on the basis of the ground-state absorption and spontaneous-fluorescence spectra. For all of these dyads in PhCN except ***o*-PMI(OR)-aep-Zn**, the spectra (due to Zn* or Fb*) at 50 ps then decay uniformly and partially by 2 ns (Figure 6H, dotted and dashed lines) and then to the 3.9 ns limit of the measurement. This behavior reflects the ~2 ns lifetime of Zn* or ~13 ns lifetime of Fb* obtained from fluorescence decays (Table 3).

The only exception to the behavior for the diarylethyne-linked dyads in PhCN described above is found in the spectra at times longer than 50 ps for ***o*-PMI(OR)-aep-Zn** in PhCN. In that case, the spectrum at 2 ns (Figure 6H, solid line) is markedly different from the others. In particular, the spectrum shows a relatively broad but pronounced absorption band at ~620 nm along with perylene bleaching (520 nm) and porphyrin bleaching (550 nm) but no porphyrin stimulated emission (e.g., 670 nm). This spectrum is assigned to the electron-transfer product state $PMI^- Zn^+$, as is described in more detail below along with the kinetics for formation and decay of this state.

3. Global Kinetic Analysis for Dyads Exhibiting No Electron-Transfer Quenching. For all of the cases except ***o*-PMI(OR)-aep-Zn** in PhCN (described in the next subsection), global analysis for each dyad/solvent was performed on the data subset encompassing 510−680 nm and −20 to 200 ps using the

TABLE 5: Summary of Kinetic Data for the Perylene−Porphyrin Dyads

		observed time constants[a]		calculated rate constants[b]	
dyad	solvent	τ_1 (ps)	τ_2 (ps)	$(k_{ENT1})^{-1}$ (ps)	$(k_{ENT2})^{-1}$ (ps)
***o*-PMI(OR)-aep-Zn**	toluene	3.1	15	7.5	15
	PhCN	2.3	15	3.6	15
***m*-PMI(OR)-aep-Zn**	toluene	3.0	16	6.9	16
	PhCN	2.8	15	5.0	15
***p*-PMI(OR)-aep-Zn**	toluene	2.7	9.7	5.5	9.7
	PhCN	1.4	7.2	1.8	7.2
***p*-PMI-aep-Zn**	toluene	nr[c]	4.5	nr[c]	4.5
	PhCN	1.8	3.5	2.5	3.5
***p*-PMI(OR)$_3$-aep-Zn**	toluene	1.4	6.2	2.0	6.2
	PhCN	1.9	7.2	2.7	7.2

[a] Time constants measured for the dyad by transient absorption spectroscopy. Time constant τ_1 reflects the decay of the unrelaxed (upper) perylene singlet excited state (PMI**) by energy transfer in competition with electronic/conformational/vibrational relaxation to the lowest excited state (PMI*), and τ_2 reflects decay of PMI* by energy transfer competing with the perylene intrinsic (monomer-like) decay pathways (fluorescence, internal conversion, and intersystem crossing); see Figure 8. [b] The value of k_{ENT1} is obtained using the formula $k_{ENT1} = (\tau_1)^{-1} - k_{rel}$, where the value of k_{rel} is the inverse of the measured time for PMI** → PMI* relaxation for the relevant perylene monomer given in Table 4. The value of k_{ENT2} is obtained using the formula $k_{ENT2} = (\tau_2)^{-1} - (\tau_{per}^{mon})^{-1}$, where τ_{per}^{mon} is the PMI* lifetime of the relevant perylene monomer given in Table 3. [c] A fast kinetic component is not resolved.

convolution of the instrument response with the dual-exponential function $A_1 \exp(-t/\tau_1) + A_2 \exp(-t/\tau_2) + C$. These cases are ***m*-PMI(OR)-aep-Zn**, ***p*-PMI(OR)-aep-Zn**, ***p*-PMI-aep-Zn**, ***p*-PMI(OR)$_3$-aep-Zn**, and ***o*-PMI(OR)-aep-Fb** in toluene and in PhCN, and ***o*-PMI(OR)-aep-Zn** in toluene. A representative kinetic profile for the latter case is shown in Figure 3C.

The dual-exponential fits to the data set for a given dyad/solvent give a fast component with a time constant (τ_1) that ranges from 1.4 to 3.1 ps and a slower component with a time constant (τ_2) in the range 3.5−24 ps (Table 5). For dyad ***o*-PMI(OR)-aep-Zn** in toluene, the spectra of the preexponential-amplitude factors A_1 and A_2 associated with the two lifetime components ($\tau_1 = 3.1$ ps, $\tau_2 = 15$ ps) and the constant asymptote C are shown in Figure 7A; such spectra are referred to as "amplitude" or "decay-associated" spectra. [Note that a negative feature ($\Delta A < 0$) in these (preexponential) amplitude spectra (also known as decay-associated spectra) reflects either the decay of a bleaching or the growth of an excited-state absorption, and similarly a positive feature reflects either the growth of a bleaching or decay of an excited-state absorption.] Figure 7C,D gives static optical data for the benchmark perylene and porphyrin monomers for comparison. Like the measured 0.5 ps spectrum for this dyad (Figure 6A, solid line), the A_1 amplitude spectrum (Figure 7A, red circles) is basically identical to the 0.5 ps spectrum for the benchmark monomer **PMI(OR)** in toluene (Figure 2A, solid line) assigned to PMI**. Similarly, the A_2 amplitude spectrum for the dyad (Figure 7A, blue squares) is basically identical to the 20 ps spectrum for **PMI(OR)** (Figure 2A, dashed line). The A_2 spectrum shows a net blue shift in the key features from the A_1 spectrum and is assigned to PMI*. Both the A_1 and A_2 amplitude spectra contain bleaching of the perylene ground-state absorption (Figure 7C, black line) at wavelengths <560 nm, consistent with the assignment to perylene-associated excited states. The C amplitude spectrum

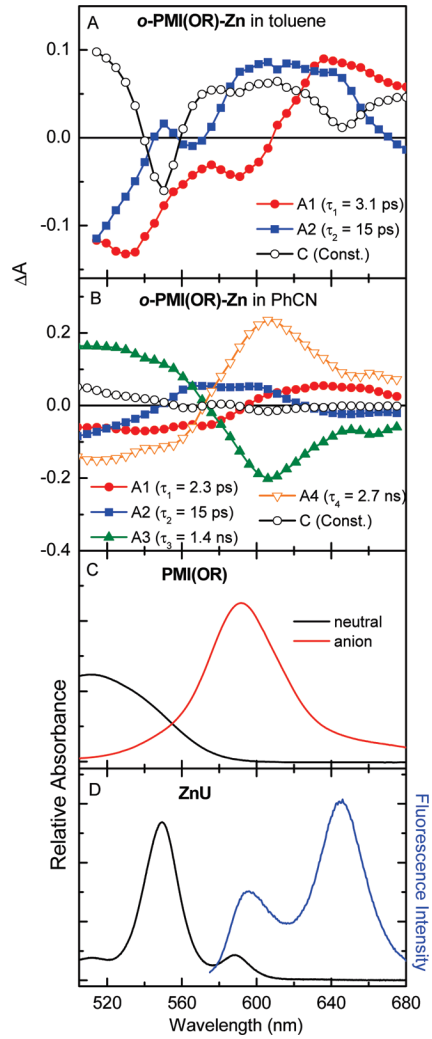

Figure 7. Amplitude spectra obtained from global analysis of the time evolution of the absorbance difference spectra (see Figure 6) for dyad ***o*-PMI(OR)-aep-Zn** in toluene (A) or PhCN (B). (C) Ground state absorption features for the perylene monomer **PMI(OR)** (black) and its π-anion radical (red) in PhCN. (D) Ground state absorption (black) and fluorescence (blue) features for porphyrin monomer **ZnU** in toluene.

(Figure 7A, open black circles) has the characteristics expected for Zn*. These features include bleaching of the Q(1,0) ground-state absorption band at 550 nm (Figure 7D, black line), Q(0,1) stimulated emission at ~650 nm that coincides with the corresponding band in the spontaneous fluorescence spectrum (Figure 7D, blue line), and a small combined Q(0,0) bleaching plus stimulated-emission feature at ~580 nm. The C component has not decayed appreciably by 200 ps (and is treated as a constant on this time scale in this analysis) consistent with the 2.4 ns Zn* lifetime obtained using fluorescence methods (Table 3). The same analysis applies to ***m*-PMI(OR)-aep-Zn**, ***p*-PMI(OR)-aep-Zn**, ***p*-PMI-aep-Zn**, ***p*-PMI(OR)$_3$-aep-Zn**, and ***o*-PMI(OR)-aep-Fb** in toluene and in PhCN. The only differences are in the τ_1 and τ_2 values, which are listed in the fifth and sixth columns of Table 5.

Analysis of the photodynamics in these dyads is facilitated by use of the kinetic model presented in Figure 8. In this model, the unrelaxed perylene excited state PMI** decays by two pathways: (i) relaxation (electronic/vibrational/conformational) to the relaxed form PMI* with rate constant k_{rel}, and (ii) energy transfer to the porphyrin with rate constant k_{ENT1}. Thus, the PMI** lifetime is $\tau_1 = (k_{rel} + k_{ENT1})^{-1}$. Subsequently, PMI*

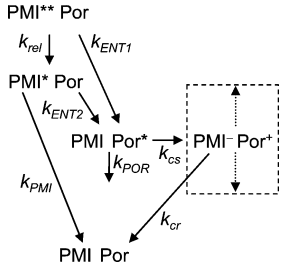

Figure 8. State diagram indicating the processes that occur in perylene−porphyrin dyads following photoexcitation. PMI** is the unrelaxed (vibrationally, conformationally, and/or electronically) singlet excited state of the perylene. PMI* is the relaxed, lowest energy singlet excited state of the perylene. The perylene monomer-like decay rate constant k_{PMI} is dominated (>90%) by fluorescence to the ground state along with some internal conversion and intersystem crossing. The porphyrin monomer-like decay rate constant k_{POR} is dominated (∼80%) by intersystem crossing to the triplet excited state with some internal conversion plus fluorescence to the ground state.

decays by two pathways: (i) decay to the ground state (and perhaps a small amount to the triplet excited state) with combined monomer-like rate constant k_{PMI} and (ii) energy transfer to the porphyrin with rate constant k_{ENT2}. Thus, the PMI* lifetime is $\tau_2 = (k_{PMI} + k_{ENT2})^{-1}$. Because Zn* (formed by perylene-to-porphyrin energy transfer) is not quenched in the diarylethyne-linked dyads being considered here (i.e., all cases except ***o*-PMI(OR)-aep-Zn** in PhCN), the perylene−porphyrin charge-separated state that would result from electron transfer either lies above Por* (Zn* or Fb* depending on the dyad) and does not form on thermodynamic grounds or lies below Por* and does not form because the electron-transfer rate is too slow compared to the monomer-like decay pathways of the excited porphyrin. This issue will be considered further in the Discussion section.

The values for k_{rel} are the inverse of the lifetimes obtained from the time-resolved spectral studies of the benchmark perylenes (Table 4). The values for k_{PMI} are determined from decay of fluorescence from the benchmark monomer [∼$(5\ ns)^{-1}$; Table 3]. These values for k_{rel} and k_{PMI}, the values of τ_1 and τ_2 derived from the global analysis (Table 5), and the formulas given above allow calculation of the rate constants k_{ENT2} and k_{ENT1} depicted in Figure 8. For example, for ***o*-PMI(OR)-aep-Zn** in toluene, substitution into the expression for the PMI** decay, $\tau_1 = (k_{rel} + k_{ENT1})^{-1}$, gives (3.1 ps) = $[(5.3\ ps)^{-1} + k_{ENT1}]^{-1}$, from which $k_{ENT1} = (7.5\ ps)^{-1}$ is obtained. These values indicate that ∼40% of the PMI** decay occurs by energy transfer to the porphyrin (producing Zn*) and the other ∼60% of the PMI** decay occurs by relaxation to PMI*. Substitution into the expression for the PMI* decay, $\tau_2 = (k_{PMI} + k_{ENT2})^{-1}$, gives (15 ps) = $[(4.8\ ns)^{-1} + k_{ENT2}]^{-1}$, from which $k_{ENT2} \approx (15\ ps)^{-1}$ is obtained. These values indicate that >99% of the PMI* decay occurs by energy transfer to the zinc porphyrin. The values of the energy-transfer rate constants obtained in this manner for ***o*-PMI(OR)-aep-Zn** in toluene are listed in the last two columns of Table 5. The same is true for the other diarylethyne-linked dyads in toluene or PhCN. The only exception is ***p*-PMI-aep-Zn** in toluene, for which a fast (τ_1) kinetic component (PMI** decay) in the dyad could not be resolved. For the latter case, the τ_2 lifetime of 4.5 ps reflects essentially quantitative energy transfer from PMI* to the porphyrin to produce Zn*, in keeping with the findings on the other diarylethyne-linked dyads.

4. Global Kinetic Analysis for o-PMI(OR)-aep-Zn in PhCN. The one case not covered in the previous subsection is ***o*-PMI(OR)-aep-Zn** in PhCN. This dyad has a transient-absorption spectrum at 2 ns (Figure 6H, solid line) that differs substantially from the other cases (including the same dyad in toluene) and can simply be ascribed to Zn*. For this case, global analysis was performed on the data set encompassing 510−680 nm and −20 ps to 3.9 ns using the convolution of the instrument response with the multiexponential function $A_1 \exp(-t/\tau_1) + A_2 \exp(-t/\tau_2) + A_3 \exp(-t/\tau_3) + A_4 \exp(-t/\tau_4) + C$. The value of τ_3 was fixed at the 1.4 ns Zn* lifetime determined from fluorescence decay (Table 3), thereby eliminating one free parameter in the fit. The time constants returned from the global fits are $\tau_1 = 2.3$ ps, $\tau_2 = 15$ ps, and $\tau_4 = 2.7$ ns. A representative kinetic profile for the latter case is shown in Figure 3B.

In analogy with the analysis for the other cases given above, the kinetic components for ***o*-PMI(OR)-aep-Zn** in PhCN with lifetimes τ_1 and τ_2 are assigned to PMI** and PMI*, respectively. In keeping with this assignment, the A_1 and A_2 amplitude spectra for (Figure 7B red and blue) are similar to those for the other cases (Figure 7A). The τ_1 and τ_2 values for this dyad together with the values for k_{rel} and k_{PMI} for the benchmark compounds gives $k_{ENT1} = (3.6\ ps)^{-1}$ and $k_{ENT2} = (15\ ps)^{-1}$ for the rate constants for energy transfer from PMI** and PMI*, respectively, to Zn*.

The Zn* lifetime of 1.4 ns for ***o*-PMI(OR)-aep-Zn** in PhCN is shorter than the value of 2.0 ns for the **ZnU** reference porphyrin in this solvent (Table 3), which is consistent with some electron-transfer quenching. On the basis of the redox potentials described above, the lowest energy electron-transfer product would be $PMI^- Zn^+$. This state must lie below (or slightly above and thermally accessible from) Zn* in this case (Figure 8). The $\tau_3 = 1.4$ ns kinetic component in the global analysis reflects the decay of Zn* and has the spectral characteristics expected for formation of $PMI^- Zn^+$. The A_3 amplitude spectrum (Figure 7B, green triangles) is well represented by subtraction of the ground-state absorption spectrum of the **PMI(OR)** monomer (Figure 7C, black line) from the spectrum for the **PMI(OR)** anion prepared electrochemically (Figure 7C, red line). Expressed in different terms, the negative feature at 620 nm in the A_3 amplitude spectrum represents formation of the perylene anion band, and the positive feature at wavelengths <560 nm represents growth of bleaching of the perylene ground-state absorption. Neither of these features is present in the measured absorption difference spectra at earlier times, which are due to Zn* [e.g., 50 ps spectrum in Figure 6G (solid line)].

Clear features associated with the zinc porphyrin in the A_3 amplitude spectrum owing to the PMI Zn* → $PMI^- Zn^+$ are not observed. This is expected because the porphyrin bleaching present in the measured Zn* spectrum (e.g., 570 nm in Figure 6G, solid) does not change appreciably as $PMI^- Zn^+$ forms (e.g., 570 nm in Figure 6H, solid line). This observation follows because any Zn* that does not lead to $PMI^- Zn^+$ (the yield will be derived below) will decay by the normal Zn* monomer-like pathways, namely, ∼80% formation of the excited triplet state Zn^T, which also exhibits ground-state bleaching, with little ground-state recovery (by fluorescence and internal conversion). Thus, the PMI Zn* → $PMI^- Zn^+$ electron-transfer process is expected to show little net signal change associated with porphyrin bleaching, and thus little contribution to the preexponential-factor amplitude spectrum. The features associated with decay of the Zn* stimulated emission as $PMI^- Zn^+$ forms overlap with the formation of the perylene anion band and are obscured. Once formed, the $PMI^- Zn^+$ state decays by charge recombination to give the ground state, with the $\tau_4 = 2.7$ ns lifetime obtained from the global analysis. The A_4 amplitude

spectrum (Figure 7B, open orange triangles) is essentially a mirror image of that associated with the formation of this state from Zn* (Figure 7B, closed green triangles). This relationship is that expected on the basis of the spectral analysis given above.

The one aspect of the photophysics of ***o*-PMI(OR)-aep-Zn** in PhCN that has not been discussed concerns the rate constant (k_{ET}) and yield (Φ_{ET}) for the PMI Zn* → PMI^- Zn^+ electron-transfer process. These values can be calculated from the excited-state lifetimes for this dyad and the **ZnU** monomer (Table 3) as follows: $k_{ET} = (1.4\ ns)^{-1} - (2.0\ ns)^{-1} = (4.7\ ns)^{-1}$ and $\Phi_{ET} = k_{ET}$ (1.4 ns) = $(4.7\ ns)^{-1}$ (1.4 ns) = 0.3. Thus, although electron-transfer quenching of Zn* occurs, the yield is only 30%.

E. Photophysical Properties of PMI(OR)$_2$-ep-Zn. All of the dyads described above contain a diarylethyne linker connected to the *N*-imide position of the perylene. These dyads all have absorption spectra that are basically the composite of those of the reference perylene and porphyrin (e.g., Figure 5). The situation is different for dyad **PMI(OR)$_2$-ep-Zn**, in which the ethyne moiety of the phenylethyne linker is attached to the C9 position of the perylene core (Chart 4). In this case, substantial deviations from the ground-state absorption spectra of the component parts are found. These differences are analogous to those found previously and described above for **PMI-ep-Zn** (Chart 3).[27] These effects reflect the very strong linker-mediated perylene−porphyrin electronic interactions.

The porphyrin fluorescence yield of **PMI(OR)$_2$-ep-Zn** (0.070) in toluene (using excitation of perylene or porphyrin) is about twice that of isolated porphyrin **ZnU** (Table 3), although the Zn* lifetime is the same (2.4 ns). We have seen similar effects in prior studies of phenylethyne-linked porphyrins, which can be attributed to a perturbed porphyrin radiative rate constant (k_f) as a result of the linker-mediated electronic coupling with the perylene. That Φ_f is affected much more strongly than τ_S follows from the formulas for these two quantities: $\Phi_f = k_f/(k_f + k_{IC} + k_{ISC})$ and $\tau_S = 1/(k_f + k_{IC} + k_{ISC})$, where k_{IC} and k_{ISC} are the rate constants for decay of the singlet excited state by internal conversion to the ground state and intersystem crossing to the triplet excited state, respectively. Because τ_S is dominated by k_{ISC}, a 2-fold perturbation in k_f has little effect. However, a 2-fold perturbation in k_f alters Φ_f by about 2-fold.

The τ_S for **PMI(OR)$_2$-ep-Zn** in toluene remains at the value of 2.4 ns found for **ZnU**, consistent with essentially no quenching of Zn* in the dyad compared to the isolated porphyrin. Thus, the incorporation of the 1- and 6-aryloxy groups on the perylene in this dyad to enhance solubility has not had a deleterious effect on the porphyrin photophysics, at least in nonpolar media. However, the situation is dramatically different for **PMI(OR)$_2$-ep-Zn** in PhCN. Now the fluorescence yield and Zn* lifetime are both substantially reduced (Table 3). The Zn* lifetime in this case is so short that it was determined by transient absorption measurements, as described in the following.

Figure 9A gives representative time-resolved absorption spectra for **PMI(OR)$_2$-ep-Zn** in PhCN acquired using excitation of the perylene at 490 nm. The spectrum at 0.5 ps after excitation is dominated by Zn*. This is evidenced by the Q(1,0) bleaching at 570 nm and the combined Q(0,0) bleaching and stimulated emission at ~620 nm. Thus, energy transfer from the excited perylene (PMI** and PMI*) to the zinc porphyrin (Figure 8) occurs in <0.5 ps. By 8 ps, bleaching in the perylene absorption at wavelengths <560 nm has developed, the Q-band bleachings of the zinc porphyrin remain, and a broad absorption feature centered at ~700 nm has developed. We interpret the latter as

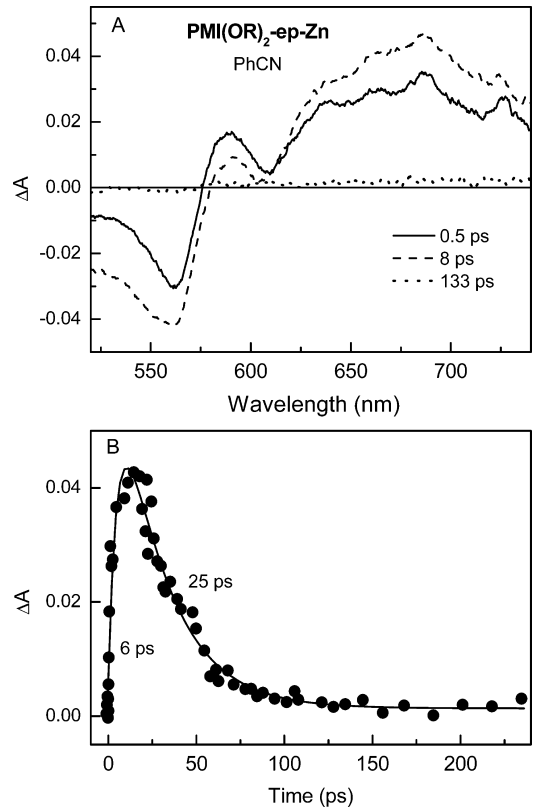

Figure 9. Representative time-resolved absorbance difference spectra (A) and kinetic profile at 700 nm (B) for dyad **PMI(OR)$_2$-ep-Zn** obtained using 130 fs excitation flashes at 490 nm. The fit in part B represents the convolution of the instrument response plus two exponentials plus a constant asymptote, giving the time constants indicated.

the perylene anion, which is red-shifted from its position at ~620 nm for **PMI(OR)** in Figure 7C due primarily to the attachment of the ethyne group to the C9 position of perylene unit. Thus, the 8 ps spectrum for **PMI(OR)$_2$-ep-Zn** in PhCN (Figure 9A, dashed line) is assigned to the electron-transfer product PMI^- Zn^+. This state has decayed by 133 ps (Figure 9A, dotted line). A representative kinetic profile is shown in Figure 9B. Analysis of such kinetic traces across the spectral region shown in Figure 9A gives time constants of 6 ± 1 ps (Zn* lifetime) and 25 ± 3 ps (PMI^- Zn^+). Compared to the Zn* lifetime of 2 ns in the benchmark porphyrin, the 6 ps lifetime in this dyad indicates that electron transfer to the perylene is essentially quantitative for **PMI(OR)$_2$-ep-Zn** in PhCN.

IV. Discussion

A. Molecular Design. Each perylene employed in this study is a monoimide construct. The monoimide derivatives were chosen over the bisimides because the former are less prone to electron-transfer quenching reactions.[27,29] One dyad, ***p*-PMI-aep-Zn**, incorporates a diarylethyne linker which joins the perylene and porphyrin via the *p*-position at the two ends of the linker. This linker motif was chosen because it should afford diminished through-bond electronic communication, thereby suppressing electron-transfer quenching reactions. Another dyad, **PMI(OR)$_2$-ep-Zn**, utilizes an ethynylphenyl linker at the C9 position of the perylene (which enhances electronic communication). For this perylene, two aryloxy substituents were incorporated both to enhance solubility and to render the chromophore more electron-rich and less susceptible to excited-state reduction with the adjoining porphyrin. Two other dyads,

***p*-PMI(OR)-aep-Zn** and ***p*-PMI(OR)$_3$-aep-Zn**, also incorporate bis-*para* attached diarylethyne linkers; however, these dyads bear one or three aryloxy groups attached to the perylene, respectively. In two other dyads, ***m*-PMI(OR)-aep-Zn** and ***o*-PMI(OR)-aep-Zn**, linker attachment to the porphyrin is at the *meso*- or *ortho*-position of the phenyl group of the diarylethyne linker. These two linkers also contain a single aryloxy group at the C9 position of the perylene. Again, the C9 aryloxy group was incorporated in an effort both to increase solubility and to render the perylene less susceptible to excited-state reduction with the adjoining porphyrin.

The *m*- and *o*-linked dyads differ from the *p*-linked dyads in that the perylene lies out of the plane of the porphyrin. An intriguing possibility is that the architectures of the *m*- and *o*-linked dyads could suppress cofacial aggregation of the porphyrins, thereby affording increased solubility compared with that of the porphyrin alone. While the solubility of the dyads is of little interest, poor solubility often is a major limitation in the synthesis and characterization of larger multipigment arrays. Thus, the *m*- and *o*-linked dyads were of interest as possible motifs that could provide advantageous light-harvesting and solubility features upon incorporation in larger constructs. In this regard, a set of organic-soluble *m*-linked perylene−porphyrin light-harvesting rods has been prepared by oligomerization of the corresponding perylene−porphyrin monomeric unit.[31]

B. Efficient Energy Transfer in the Absence of Electron-Transfer Quenching. In all of the diarylethyne-linked perylene−porphyrin dyads investigated herein (Charts 4 and 5), energy transfer from the perylene to the porphyrin (zinc chelate or free base) is facile and efficient. Even starting in the unrelaxed perylene excited state PMI**, energy transfer to the porphyrin is sufficiently fast (∼2−8 ps) that it has a yield of about 50%. Energy transfer for the relaxed excited state PMI* is also rapid (∼5−25 ps) and effectively quantitative because it is competing with the monomer-like decay time of ∼5 ns. Once the energy reaches the porphyrin, no quenching is observed for all but one of the diarylethyne-linked perylene−porphyrin dyads studied, and that quenching occurs only to a modest degree in PhCN. That one exception is ***o*-PMI(OR)-aep-Zn** in PhCN, which is discussed further below. Thus, all of these dyad motifs are excellent constructs as ancillary light-harvesting units in synthetic or biohybrid constructs for solar-energy conversion in both nonpolar and highly polar media. The fact that electron-transfer quenching does not occur even in highly polar media is quite favorable for many applications, such as solution-based or solid-state solar cells where the medium may have a high dielectric to enhance ion mobility or charge transfer.

C. Modest Electron-Transfer Quenching for *o*-PMI(OR)-aep-Zn in PhCN. The one case investigated where a perylene−porphyrin dyad exhibits quenching of the porphyrin excited state compared to the isolated porphyrin is ***o*-PMI(OR)-aep-Zn** in PhCN. For this dyad, the electron-transfer product state generically denoted PMI$^-$ Por$^+$ in Figure 8 (PMI$^-$ Zn$^+$ in this case) must lie either below the excited porphyrin generically denoted Por* in Figure 8 (Zn* in this case) or within thermal energy (kT) above Por*. For the other diarylethyne-linked dyads, the exact energetic positioning of PMI$^-$ Por$^+$ relative to Por* in PhCN is not entirely clear. The most straightforward interpretation for the absence of electron transfer is that PMI$^-$ Por$^+$ is above Por*. Regardless of the details of the energetics of PMI$^-$ Por$^+$ versus Por* in PhCN, it is clear that the former state lies higher in energy in toluene. A possible reason why PMI$^-$ Por$^+$ might lie lower in energy for ***o*-PMI(OR)-aep-Zn** in PhCN compared to the other dyads, such as ***p*-PMI(OR)-aep-Zn** and ***m*-PMI(OR)-aep-Zn**, is that the closer perylene−porphyrin distance (Chart 4) would give a larger Coulomb interaction ($-e^2/\varepsilon R$). [Here, e is the electron charge, ε is the dielectric constant of the solvent, and R is the separation of the charges (e.g., perylene−porphyrin center-to-center distance).] However, the magnitude of this effect is unclear.

Another reason why electron-transfer quenching may occur for ***o*-PMI(OR)-aep-Zn** and not the other dyads such as ***p*-PMI(OR)-aep-Zn** and ***m*-PMI(OR)-aep-Zn** in PhCN is that the closer distance between the perylene and the porphyrin using the *o*-linkage motif would give a larger solvent reorganization energy, in addition to a possible difference in the free energy change for the reaction. The Franck−Condon factor and thus the rate constant for electron-transfer quenching is dictated by the relationship between these two quantities, which in turn reflects the relationship between the potential energy surfaces of Zn* and PMI$^-$ Zn$^+$. Furthermore, the perylene and porphyrin may become sufficiently close in ***o*-PMI(OR)-aep-Zn** to allow substantial orbital overlap. In this case, this "through-space" interaction would enhance the electron transfer compared to the other connection motifs, wherein only linker-mediated "through-bond" transfer can occur.

In the analysis presented in the Results section, it was found that the PMI Zn* → PMI$^-$ Zn$^+$ electron-transfer process for ***o*-PMI(OR)-aep-Zn** in PhCN is rather slow, with a rate constant of (4.7 ns)$^{-1}$. When compared to the normal monomer-like combined decay rate of (2.0 ns)$^{-1}$ for Zn* in this medium, this accounts for the modest yield of 0.3 for the process. Thus, although quenching of Zn* is observed for ***o*-PMI(OR)-aep-Zn** in the highly polar medium PhCN, the extent is only 30% and leaves a modestly long (1.4 ns) excited-state lifetime for utilization of the harvested light energy. Additionally, this modest quenching can be readily eliminated. For example, the quenching does not occur for this same dyad in toluene because the reduced solvent stabilization moves the electron-transfer product state PMI$^-$ Zn$^+$ to higher energy. Similarly, quenching is not observed for ***o*-PMI(OR)-aep-Fb** in either toluene or PhCN because the free base porphyrin is harder to oxidize than the zinc porphyrin.

D. Phenylethyne-Linked Dyads. The direct attachment of the ethyne group of the phenylethyne linker to the perylene C9 position (e.g., **PMI(OR)$_2$-ep-Zn**) greatly increases the rate of energy transfer from perylene to porphyrin compared to use of a diarylethyne linker attached to the *N*-imide of the perylene (e.g., ***p*-PMI(OR)-ep-Zn**), namely, <0.5 ps versus 5−25 ps depending on the dyad. Because energy transfer is competing with an ∼5 ns inherent lifetime for the excited perylene, the energy-transfer yield is essentially quantitative in both systems. Thus, the enhanced rates for the phenylethyne linker have not paid a dividend in terms of yield compared to the diarylethyne linker. The net cost of increasing the energy-transfer rate is that the perylene ethyne attachment makes the perylene easier to reduce, and thus the associated dyads more susceptible to electron-transfer quenching. We had observed this behavior previously for **PMI-ep-Zn** (Chart 3)[27] and found that the same is true here for **PMI(OR)$_2$-ep-Zn**, in which the aryloxy groups were incorporated for enhanced solubility. Both systems are excellent light-harvesting motifs in nonpolar media such as toluene but undergo ultrafast electron-transfer quenching of the excited porphyrin followed by rapid (tens of picoseconds) charge recombination to give back the ground state in highly polar media such as PhCN.

V. Conclusions

The studies described herein have identified perylene−porphyrin dyads that represent excellent motifs for use in light-harvesting architectures. The dyads employ diarylethyne linkers with attachment to the *N*-imide position of the perylene-monomide. These constructs give rapid and quantitative perylene-to-porphyrin energy transfer and long porphyrin excited-state lifetimes that are unchanged from those in the isolated porphyrin. The incorporation of up to three aryloxy groups to impart increased solubility to the perylene has the added benefit of making the dyad somewhat less prone to electron-transfer quenching. A diarylethyne-linked dyad that has close approach of the perylene and porphyrin due to the use of *o*-positions of an aryl ring of the linker also has excellent light-harvesting characteristics in nonpolar media but suffers from electron-transfer quenching in polar media. A construct that utilizes a phenylethyne linker attached to the C9 position of the perylene gives even faster (<0.5 ps) perylene-to-porphyrin energy transfer but is also not satisfactory for light-harvesting applications due to facile electron transfer and ultrafast charge recombination in polar media. Collectively, the studies described herein provide concepts and architectures that should be useful in the design of molecular solar energy conversion systems.

Acknowledgment. This work was supported by grants from the Division of Chemical Sciences, Geosciences and Biosciences Division, Office of Basic Energy Sciences, of the U.S. Department of Energy to D.F.B. (DE-FG02-05ER15660), D.H. (DE-FG02-05ER15661), and J.S.L. (DE-FG02-96ER14632).

Supporting Information Available: Transient absorption spectra of perylene monomers, absorption and fluorescence spectra of perylene monomers in a variety of solvents, and a table of solvent properties. This material is available free of charge via the Internet at http://pubs.acs.org.

References and Notes

(1) Holten, D.; Bocian, D. F.; Lindsey, J. S. *Acc. Chem. Res.* **2002**, *35*, 57–69.

(2) Harvey, P. D. In *The Porphyrin Handbook*; Kadish, K. M., Smith, K. M., Guilard, R., Eds.; Academic Press: San Diego, CA, 2003; Vol. 18, pp 63−250.

(3) (a) Wagner, R. W.; Lindsey, J. S. *Pure Appl. Chem.* **1996**, *68*, 1373–1380. (b) Wagner, R. W.; Lindsey, J. S. *Pure Appl. Chem.* **1998**, *70* (8), p. i.

(4) Demmig, S.; Langhals, H. *Chem. Ber.* **1988**, *121*, 225–230.

(5) Ford, W. E.; Kamat, P. V. *J. Phys. Chem.* **1987**, *91*, 6373–6380.

(6) (a) Rademacher, A.; Märkle, S.; Langhals, H. *Chem. Ber.* **1982**, *115*, 2927–2934. (b) Ebeid, E.-Z. M.; El-Daly, S. A.; Langhals, H. *J. Phys. Chem.* **1988**, *92*, 4565–4568.

(7) Langhals, H. *Chem. Ber.* **1985**, *118*, 4641–4645.

(8) Würthner, F. *Chem. Commun.* **2004**, 1564–1579.

(9) Langhals, H. *Helv. Chim. Acta* **2005**, *88*, 1309–1343.

(10) Herrmann, A.; Müllen, K. *Chem. Lett.* **2006**, *35*, 978–985.

(11) Chen, Z.; Lohr, A.; Saha-Möller, C. R.; Würthner, F. *Chem. Soc. Rev.* **2009**, *38*, 564–584.

(12) Mativetsky, J. M.; Kastler, M.; Savage, R. C.; Gentilini, D.; Palma, M.; Pisula, W.; Müllen, K.; Samori, P. *Adv. Funct. Mater.* **2009**, *19*, 2486–2494.

(13) Langhals, H. *Nachr. Chem., Tech. Lab.* **1980**, *28*, 716–718.

(14) Quante, H.; Müllen, K. *Angew. Chem., Int. Ed. Engl.* **1995**, *34*, 1323–1325.

(15) Langhals, H.; Demmig, S.; Huber, H. *Spectrochim. Acta* **1988**, *44A*, 1189–1193.

(16) Adachi, M.; Murata, Y.; Nakamura, S. *J. Phys. Chem.* **1995**, *99*, 14240–14246.

(17) Gosztola, D.; Niemczyk, M. P.; Wasielewski, M. R. *J. Am. Chem. Soc.* **1998**, *120*, 5118–5119.

(18) Hayes, R. T.; Wasielewski, M. R.; Gosztola, D. *J. Am. Chem. Soc.* **2000**, *122*, 5563–5567.

(19) van der Boom, T.; Hayes, R. T.; Zhao, Y.; Bushard, P. J.; Weiss, E. A.; Wasielewski, M. R. *J. Am. Chem. Soc.* **2002**, *124*, 9582–9590.

(20) Ahrens, M. J.; Kelley, R. F.; Dance, Z. E. X.; Wasielewski, M. R. *Phys. Chem. Chem. Phys.* **2007**, *9*, 1469–1478.

(21) Kelley, R. F.; Shin, W. S.; Rybtchinski, B.; Sinks, L. E.; Wasielewski, M. R. *J. Am. Chem. Soc.* **2007**, *129*, 3173–3181.

(22) Odom, S. A.; Kelley, R. F.; Ohira, S.; Ensley, T. R.; Huang, C.; Padilha, L. A.; Webster, S.; Coropceanu, V.; Barlow, S.; Hagan, D. J.; van Stryland, E. W.; Brédas, J.-L.; Anderson, H. L.; Wasielewski, M. R.; Marder, S. R. *J. Phys. Chem. A* **2009**, *113*, 10826–10832.

(23) Tasior, M.; Gryko, D. T.; Shen, J.; Kadish, K. M.; Becherer, T.; Langhals, H.; Ventura, B.; Flamigni, L. *J. Phys. Chem. C* **2008**, *112*, 19699–19709.

(24) Miller, M. A.; Lammi, R. K.; Prathapan, S.; Holten, D.; Lindsey, J. S. *J. Org. Chem.* **2000**, *65*, 6634–6649.

(25) Prathapan, S.; Yang, S. I.; Seth, J.; Miller, M. A.; Bocian, D. F.; Holten, D.; Lindsey, J. S. *J. Phys. Chem. B* **2001**, *105*, 8237–8248.

(26) Yang, S. I.; Prathapan, S.; Miller, M. A.; Seth, J.; Bocian, D. F.; Lindsey, J. S.; Holten, D. *J. Phys. Chem. B* **2001**, *105*, 8249–8258.

(27) Yang, S. I.; Lammi, R. K.; Prathapan, S.; Miller, M. A.; Seth, J.; Diers, J. R.; Bocian, D. F.; Lindsey, J. S.; Holten, D. *J. Mater. Chem.* **2001**, *11*, 2420–2430.

(28) Ambroise, A.; Kirmaier, C.; Wagner, R. W.; Loewe, R. S.; Bocian, D. F.; Holten, D.; Lindsey, J. S. *J. Org. Chem.* **2002**, *67*, 3811–3826.

(29) Kirmaier, C.; Yang, S. I.; Prathapan, S.; Miller, M. A.; Diers, J. R.; Bocian, D. F.; Lindsey, J. S.; Holten, D. *Res. Chem. Intermed.* **2002**, *28*, 719–740.

(30) Tomizaki, K.-Y.; Loewe, R. S.; Kirmaier, C.; Schwartz, J. K.; Retsek, J. L.; Bocian, D. F.; Holten, D.; Lindsey, J. S. *J. Org. Chem.* **2002**, *67*, 6519–6534.

(31) Loewe, R. S.; Tomizaki, K.-Y.; Youngblood, W. J.; Bo, Z.; Lindsey, J. S. *J. Mater. Chem.* **2002**, *12*, 3438–3451.

(32) Loewe, R. S.; Tomizaki, K.-y.; Chevalier, F.; Lindsey, J. S. *J. Porphyrins Phthalocyanines* **2002**, *6*, 626–642.

(33) Muthukumaran, K.; Loewe, R. S.; Kirmaier, C.; Hinden, E.; Schwartz, J. K.; Sazanovich, I. V.; Diers, J. R.; Bocian, D. F.; Holten, D.; Lindsey, J. S. *J. Phys. Chem. B* **2003**, *107*, 3431–3442.

(34) Kirmaier, C.; Hinden, E.; Schwartz, J. K.; Sazanovich, I. V.; Diers, J. R.; Muthukumaran, K.; Taniguchi, M.; Bocian, D. F.; Lindsey, J. S.; Holten, D. *J. Phys. Chem. B* **2003**, *107*, 3443–3454.

(35) Tomizaki, K.-y.; Thamyongkit, P.; Loewe, R. S.; Lindsey, J. S. *Tetrahedron* **2003**, *59*, 1191–1207.

(36) Hofkens, J.; Latterini, L.; De Belder, G.; Gensch, T.; Maus, M.; Vosch, T.; Karni, Y.; Schweitzer, G.; De Schryver, F. C.; Hermann, A.; Müllen, K. *Chem. Phys. Lett.* **1999**, *304*, 1–9.

(37) Wagner, R. W.; Johnson, T. E.; Lindsey, J. S. *J. Am. Chem. Soc.* **1996**, *118*, 11166–11180.

(38) Lindsey, J. S.; Prathapan, S.; Johnson, T. E.; Wagner, R. W. *Tetrahedron* **1994**, *50*, 8941–8968.

(39) Wagner, R. W.; Johnson, T. E.; Li, F.; Lindsey, J. S. *J. Org. Chem.* **1995**, *60*, 5266–5273.

(40) Strachan, J.-P.; Gentemann, S.; Seth, J.; Kalsbeck, W. A.; Lindsey, J. S.; Holten, D.; Bocian, D. F. *J. Am. Chem. Soc.* **1997**, *119*, 11191–11201.

(41) Hindin, E.; Forties, R. A.; Loewe, R. S.; Ambroise, A.; Kirmaier, C.; Bocian, D. F.; Lindsey, J. S.; Holten, D.; Knox, R. S. *J. Phys. Chem. B* **2004**, *108*, 12821–12832.

(42) del Rosario Benites, M.; Johnson, T. E.; Weghorn, S.; Yu, L.; Rao, P. D.; Diers, J. R.; Yang, S. I.; Kirmaier, C.; Bocian, D. F.; Holten, D.; Lindsey, J. S. *J. Mater. Chem.* **2002**, *12*, 65–80.

(43) Kong, J.; White, C. A.; Krylov, A. I.; Sherrill, D.; Adamson, R. D.; Furlani, T. R.; Lee, M. S.; Lee, A. M.; Gwaltney, S. R.; Adams, T. R.; Ochsenfeld, C.; Gilbert, A. T. B.; Kedziora, G. S.; Rassolov, V. A.; Maurice, D. R.; Nair, N.; Shao, Y.; Besley, N. A.; Maslen, P. E.; Dombroski, J. P.; Daschel, H.; Zhang, W.; Korambath, P. P.; Baker, J.; Byrd, E. F. C.; Van Voorhis, T.; Oumi, M.; Hirata, S.; Hsu, C.-P.; Ishikawa, N.; Florian, J.; Warshel, A.; Johnson, B. G.; Gill, P. M.; Head-Gordon, M.; Pople, J. A. *J. Comput. Chem.* **2000**, *21*, 1532–1548.

(44) Felton, R. H. In *The Porphyrins*; Dolphin, D., Ed.; Academic Press: New York, 1978; Vol. V, pp 53−125.

(45) Hofkens, J.; Latterini, L.; De Belder, G.; Gensch, T.; Maus, M.; Vosch, T.; Karni, Y.; Schweitzer, G.; De Schryver, F. C.; Hermann, A.; Müllen, K. *Chem. Phys. Lett.* **1999**, *304*, 1–9.

(46) Yang, S. I.; Seth, J.; Strachan, J.-P.; Gentemann, S.; Kim, D.; Holten, D.; Lindsey, J. S.; Bocian, D. F. *J. Porphyrins Phthalocyanines* **1999**, *3*, 117–147.

(47) Li, F.; Yang, S. I.; Ciringh, Y.; Seth, J.; Martin, C. H., III; Singh, D. L.; Kim, D.; Birge, R. R.; Bocian, D. F.; Holten, D.; Lindsey, J. S. *J. Am. Chem. Soc.* **1998**, *120*, 10001–10017.

(48) Kee, H. L.; Kirmaier, C.; Yu, L.; Thamyongkit, P.; Youngblood, W. J.; Calder, M. E.; Ramos, L.; Noll, B. C.; Bocian, D. F.; Scheidt, W. R.; Birge, R. R.; Lindsey, J. S.; Holten, D. *J. Phys. Chem. B* **2005**, *109*, 20433–20443.

(49) Sazanovich, I. V.; Kirmaier, C.; Hindin, E.; Yu, L.; Bocian, D. F.; Lindsey, J. S.; Holten, D. *J. Am. Chem. Soc.* **2004**, *126*, 2664–2665.

(50) Basu, S. *Adv. Quantum Chem.* **1964**, *1*, 145–169.

JP910705Q